



Volume 11, Issue Suppl_1, June 2021
ISSN / eISSN: 2158-0510 / 2158-0529

IJB M

International Journal
BIOMEDICINE

Abstracts
from the Third Russian
International Conference “Cryo-
Electron Microscopy 2021:
Achievements and Prospects”

May 30 –June 2, 2021 • Moscow • Russia

IJB M

International Journal of
BIOMEDICINE



ISSN 2158-0510

Available online at
www.ijbm.org

INTERNATIONAL JOURNAL OF BIOMEDICINE

Aims and Scope: *International Journal of Biomedicine (IJBM)* publishes peer-reviewed articles on the topics of basic, applied, and translational research on biology and medicine. Original research studies, reviews, hypotheses, editorial commentary, and special reports spanning the spectrum of human and experimental and tissue research will be considered. All research studies involving animals must have been conducted following animal welfare guidelines such as the National Institutes of Health (NIH) Guide for the Care and Use of Laboratory Animals, or equivalent documents. Studies involving human subjects or tissues must adhere to the Declaration of Helsinki and Title 45, US Code of Federal Regulations, Part 46, Protection of Human Subjects, and must have received approval of the appropriate institutional committee charged with oversight of human studies. Informed consent must be obtained.

International Journal of Biomedicine endorses and behaves in accordance with the codes of conduct and international standards established by the Committee on Publication Ethics (COPE).

International Journal of Biomedicine (ISSN 2158-0510) is published four times a year by International Medical Research and Development Corp. (IMRDC), 6308, 12 Avenue, Brooklyn, NY 11219 USA

Customer Service: International Journal of Biomedicine, 6308, 12 Avenue, Brooklyn, NY 11219 USA; Tel: 1-917-740-3053; E-mail: editor@ijbm.org

Photocopying and Permissions: Published papers appear electronically and are freely available from our website. Authors may also use their published .pdf's for any non-commercial use on their personal or non-commercial institution's website. Users are free to read, download, copy, print, search, or link to the full texts of these articles for any non-commercial purpose. Articles from IJBM website may be reproduced, in any media or format, or linked to for any commercial purpose, subject to a selected user license.

Notice: No responsibility is assumed by the Publisher, Corporation or Editors for any injury and/or damage to persons or property as a matter of products liability, negligence, or otherwise, or from any use or operation of any methods, products, instructions, or ideas contained in the material herein. Because of rapid advances in the medical and biological sciences, in particular, independent verification of diagnoses, drug dosages, and devices recommended should be made. Although all advertising material is expected to conform to ethical (medical) standards, inclusion in this publication does not constitute a guarantee or endorsement of the quality or value of such product or of the claims made of it by its manufacturer.

Manuscript Submission: Original works will be accepted with the understanding that they are contributed solely to the Journal, are not under review by another publication, and have not previously been published except in abstract form. Accepted manuscripts become the sole property of the Journal and may not be published elsewhere without the consent of the Journal. A form stating that the authors transfer all copyright ownership to the Journal will be sent from the Publisher when the manuscript is accepted; this form must be signed by all authors of the article. All manuscripts must be submitted through the International Journal of Biomedicine's online submission and review website. Authors who are unable to provide an electronic version or have other circumstances that prevent online submission must contact the Editorial Office prior to submission to discuss alternate options (editor@ijbm.org).

IJB M

INTERNATIONAL JOURNAL OF BIOMEDICINE

Editor-in-Chief
Marietta Eliseyeva
New York, USA

Founding Editor
Simon Edelstein
Detroit, MI, USA

EDITORIAL BOARD

Mary Ann Lila
*North Carolina State University
Kannapolis, NC, USA*

Ilya Raskin
*Rutgers University
New Brunswick, NJ, USA*

Yue Wang
*National Institute for Viral Disease
Control and Prevention, CCDC
Beijing, China*

Nigora Srojedinova
*National Center of Cardiology
Tashkent, Uzbekistan*

Dmitriy Labunskiy
*Lincoln University
Oakland, CA, USA*

Randy Lieberman
*Detroit Medical Center
Detroit, MI, USA*

Seung H. Kim
*Hanyang University Medical Center
Seoul, South Korea*

Alexander Dreval
*M. Vladimirsky Moscow Regional
Research Clinical Institute, Russia*

Bruna Scaggiante
*University of Trieste
Trieste, Italy*

Shaoling Wu
*Qingdao University, Qingdao
Shandong, China*

Roy Beran
*Griffith University, Queensland
UNSW, Sydney, Australia*

Biao Xu
*Nanjing University
Nanjing, China*

Alexander Vasilyev
*Central Research Radiology Institute
Moscow, Russia*

Karunakaran Rohini
*AIMST University
Bedong, Malaysia*

Luka Tomašević
*University of Split
Split, Croatia*

Lev Zhivotovsky
*Vavilov Institute of General Genetics
Moscow, Russia*

Bhaskar Behera
*Agharkar Research Institute
Pune, India*

Srdan Poštić
*University School of Dental Medicine
Belgrade, Serbia*

Gayrat Kiyakbayev
*RUDN University
Moscow Russia*

Hesham Abdel-Hady
*University of Mansoura
Mansoura, Egypt*

Nikolay Soroka
*Belarusian State Medical University
Minsk, Belarus*

Boris Mankovsky
*National Medical Academy for
Postgraduate Education
Kiev, Ukraine*

Tetsuya Sugiyama
*Nakano Eye Clinic
Nakagyo-ku, Kyoto, Japan*

Alireza Heidari
*California South University
Irvine, California, USA*

Rupert Fawdry
*University Hospitals of Coventry &
Warwickshire Coventry, UK*

Igor Kireev
*AN Belozersky Inst of Physico-Chemical
Biology, Moscow State University, Russia*

Sergey Popov
*Scientific Research Institute of
Cardiology, Tomsk, Russia*

Editorial Staff

Paul Edelstein (*Managing Editor*)

Dmitriy Eliseyev (*Statistical Editor*)

Arita Muhaxhery (*Editorial Assistant*)

2017 NOBEL PRIZE IN CHEMISTRY

Jacques Dubochet
Joachim Frank
Richard Henderson



"for developing cryo-electron microscopy for the high-resolution structure determination of biomolecules in solution"

IJB M

INTERNATIONAL JOURNAL OF BIOMEDICINE

www.ijbm.org

June 2021 - Volume 11, Issue Suppl_1

CONTENTS

Abstracts From the Third Russian International Conference "Cryo-electron microscopy 2021: achievements and prospects"

ORAL ABSTRACT PRESENTATIONS

Structure of Membrane Proteins	7
EM Research Related to Medicine	8
Structure of Viruses and Chaperonins.....	9

POSTER ABSTRACT PRESENTATIONS

Advances in EM Technology and Processing.....	11
Structure of Membrane Proteins	15
Structure and Functions of the Transcription and Translation Apparatus of the Cell.....	19
EM Research Related to Medicine	25
Structure of Viruses and Chaperonins.....	31

STRUCTURE OF MEMBRANE PROTEINS

OR-1

http://dx.doi.org/10.21103/IJBM.11.Suppl_1.OR1**Condensed DNA Architecture in a Nucleoid of *Escherichia coli***Yurii Krupyanski¹, Nataliya Loiko², Olga Sokolova³¹Semenov Federal Research Center for Chemical Physics RAS, Moscow, Russia²FR Center "Fundamentals of Biotechnology" RAS, Moscow, Russia³Biological Faculty, Lomonosov Moscow State University, Moscow, Russia

Background: Bacterial genomic DNA interacts with nucleoid-associated proteins (NAPs) and is located in a highly condensed and functional organized form in the nucleoid of the cell. The structure of the bacterial nucleoid is still awaiting its determination in high resolution. However, recent intensive research showed that condensed DNA in the bacterial nucleoid has a complex, hierarchically organized structure. Such architecture may only exist as a result of dynamic structural rearrangements, which characterize actively growing bacteria. Changes in environmental conditions are perceived by bacteria as stress. In the stationary phase caused by nutrient depletion, energy production processes become inefficient. Bacteria in the stationary phase use an energy-independent mechanism for maintaining an order to protect the DNA: the creation of stable structures, like those in inanimate nature. Cells develop into dormant forms that differ significantly in the structural organization from growing cells.

Methods: Electron microscopy and synchrotron radiation diffraction studies were used to reveal distinct forms of DNA condensation in dormant *E. coli* cells.

Results: The study made it possible to find the intracellular nanocrystalline, liquid crystalline, and folded nucleosome-like DNA structures, which were observed and described for the first time.

Conclusions: The results of experiments made it possible to visualize the structures of the lower hierarchical tier of DNA compaction in the nucleoid of dormant cells. We hypothesized that the heterogeneity of bacterial cells allows for a flexible response to environmental changes and to surviving stress situations. Multiple types of DNA condensation in the same dormant *E. coli* cell increase the chances for rapid resumption of growth when conditions turn back to favorable.

Key Words: stress, DNA, condensation, structure

Research was performed within frameworks of the state tasks for FRC CP RAS #AAAA-A20-120031490003-7 and #AAAA-A19-119021490112-1

*Corresponding author: Krupyanski Yurii. E-mail: yuriifkru@gmail.com

OR-2

http://dx.doi.org/10.21103/IJBM.11.Suppl_1.OR2**The Formation of Dps-DNA Complexes under Different Conditions According to Cryo-EM and SAXS**Roman Kamyshinsky^{1,2}, Yury Chesnokov^{1,2}, Liubov Dadinova², Andrey Mozhaev^{2,3}, Alexander Vasiliev^{1,2}, Eleonora Shtykova²¹National Research Center "Kurchatov Institute," Moscow, Russia²Shubnikov Institute of Crystallography of FSRC "Crystallography and Photonics" RAS, Moscow, Russia³Shemyakin-Ovchinnikov Institute of Bioorganic Chemistry of RAS, Moscow, Russia

Background: The effect of Dps-DNA co-crystals formation, which occurs in stressed *Escherichia coli* cells exposed to extreme conditions, is well described in the literature. However, the exact mechanisms of co-crystals formation are yet to be postulated remaining largely unknown. Here we summarize the results obtained by our group over the last few years using cryo-Electron Microscopy (cryo-EM) and Small Angle X-ray Scattering (SAXS).

Methods: Samples for cryo-EM were plunge frozen in liquid ethane with Vitrobot Mark IV and studied with Titan Krios (ThermoFisher Scientific, US) cryo-EM, equipped with Falcon 2 direct electron detector, Image corrector (CEOS, Germany), and Volta phase plate.

Single Particle Analysis (SPA) and cryo-Electron Tomography (cryo-ET) studies were conducted with 300 kV accelerating voltage in low dose mode using EPU and Tomography software (ThermoFisher Scientific, US). Cryo-EM data processing was conducted using Warp, CryoSPARC, IMOD, EMAN, and Relion software packages. SAXS measurements were performed at the EMBL on the P12 BioSAXS beam line at the PETRAIII storage ring (DESY, Hamburg).

Results: In this work, Dps-DNA complex formation is thoroughly studied using complementary cryo-EM (including SPA, cryo-ET, and subtomogram averaging) and SAXS methods. The formation of individual complexes of Dps with small linear DNA fragments and the Dps-Dps interaction was visualized using cryo-EM. It was found that Dps-DNA complex remains stable under various conditions and while the addition of different ions leads to the disruption of co-crystals, the process is completely or partially reversible.

Conclusion: Recent studies conducted by our group showed that Dps-DNA co-crystals adopt triclinic or cubic crystal lattice (FEBS Lett., 2019; Biomolecules, 2020). Here we present the results on the studies of Dps interaction with small linear DNA fragments, demonstrate the effects of MgCl₂, FeSO₄, and EDTA on the Dps-DNA complex and individual Dps protein structure, discuss the influence of the temperature and time on the co-crystals.

Key Words: Dps-DNA, co-crystals, cryo-EM, SAXS

This work was supported by the Russian Science Foundation (Project № 18-74-10071).

*Corresponding author: Roman Kamyshinsky. E-mail: kamyshinsky.roman@gmail.com

OR-3

http://dx.doi.org/10.21103/IJBM.11.Suppl_1.OR3**Integrative Structural Study of the Complex of Snake Toxin WTX with $\alpha 7$ -type Nicotinic Acetylcholine Receptor**Ekaterina Lyukmanova¹, Maxim M. Zaigraev¹, Dmitrii S. Kulbatskii¹, Milita V. Kocharovskaya¹, Yury M. Chesnokov², Anton O. Chugunov¹, Mikhail P. Kirpichnikov^{1,3}, Zakhar O. Shenkarev¹¹Shemyakin-Ovchinnikov Institute of Bioorganic Chemistry, Russian Academy of Sciences, Moscow, Russia

²National Research Center "Kurchatov Institute," Moscow, Russia

³Biological Faculty, Lomonosov Moscow State University, Moscow, Russia

Background: Nicotinic acetylcholine receptors are ligand-gated ion channels present in the nervous system, epithelium, and the immune system. The $\alpha 7$ -type nicotinic receptor ($\alpha 7$ -nAChR) is a homopentameric membrane protein containing five ligand binding sites located at the interface between subunits in the extracellular domain of the receptor. $\alpha 7$ -nAChR is considered a promising target for the treatment of cancer and cognitive dysfunction in Alzheimer's disease, schizophrenia, and depression. WTX is a non-conventional three-finger neurotoxin from the *Naja kaouthia* venom inhibiting $\alpha 7$ -nAChR. WTX structure consists of three loops protruding from the "head" (core) stabilized by a system of disulfide bonds.

Methods: The complex of the $\alpha 7$ -nAChR extracellular domain with a recombinant analogue of WTX was studied by cryo-electron microscopy. The structure of the complex of full-length $\alpha 7$ -nAChR with the toxin in the membrane environment was reconstructed by in silico molecular modeling. Interaction of WTX with the lipid membrane was confirmed by NMR-spectroscopy.

Results: Analysis of electronic images confirmed the homopentameric organization of the extracellular domain with a diameter of ~ 9 nm and a height of ~ 7 nm. On the electron density map, additional regions corresponding to five WTX molecules located at the intersubunit interfaces of the domain were observed. Fitting the known spatial structures of the extracellular domain and the WTX toxin into the obtained electron density made it possible to reconstruct the structure of the complex (although with a low resolution of ~ 8 Å due to the predominant orientation of particles in the ice) and to determine the topology of the toxin-receptor interaction. It was revealed that WTX interacts with the extracellular domain of $\alpha 7$ -nAChR by the loop II, while the loop I and the toxin's head seem to interact with the surface of the lipid membrane surrounding the receptor. Model of the complex of the full-length $\alpha 7$ -nAChR receptor with WTX in the membrane environment corresponding to the neuronal membrane was constructed using computer simulation methods. Molecular dynamics for > 1500 ns confirmed the stability of the complex. The predicted membrane-active site of the WTX molecule includes residues Lys13 and Arg18. The study of WTX and its mutants Lys13Ala and Arg18Ala by NMR-spectroscopy confirmed the importance of these residues for interaction with lipid membrane.

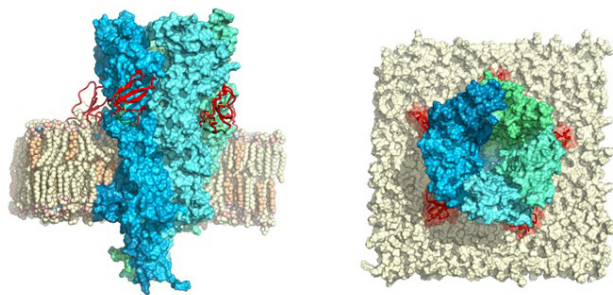


Fig. 1. The model of the complex of $\alpha 7$ -nAChR/WTX in the membrane environment. Side and top views.

Conclusions: Interaction mode of non-conventional neurotoxins with nAChR has been determined for the first time.

Key Words: three-finger toxin, $\alpha 7$ -nAChR, cryo-EM, neuronal membrane

This work was supported by the Russian Science Foundation (Project № 19-74-20163)

*Corresponding author: Ekaterina Lyukmanova. E-mail: ekaterina-lyukmanova@yandex.ru

EM RESEARCH RELATED TO MEDICINE

OR-4

http://dx.doi.org/10.21103/IJBM.11.Suppl_1.OR4

New Antibiotic Binding Site on the 30S Ribosomal Subunit

Irina M Lisevich¹, Dmitrii A. Lukianov¹, Daniel N. Wilson², Petr V. Sergiev^{1,3}, Olga A. Dontsova^{1,3,4}, Ilya A Osterman^{1,3,5}

¹Center of Life Sciences, Skolkovo Institute of Science and Technology, Skolkovo, Russia

²Institute for Biochemistry and Molecular Biology, University of Hamburg, Hamburg, Germany

³Lomonosov Moscow State University, Moscow, Russia

⁴Shemyakin-Ovchinnikov Institute of Bioorganic Chemistry, Russian Academy of Sciences, Moscow, Russia

⁵Sirius University of Science and Technology, Sochi, Russia

Background: Antibiotic resistance becomes one of the main problems of modern medicine; therefore, the development of new antibacterial compounds is absolutely necessary. The ribosome is the target for a lot of different antibiotics; there are several main binding sites on the ribosome – decoding center, peptidyl-transferase center, and ribosome exit tunnel. Modification or mutation of nucleotides in these sites could make cells resistant to structurally different antibiotics.

Methods: pDualrep2 reporter system was used for detection of the protein synthesis inhibitors in cultural broths of new soil bacteria. By means of a cell-free translation system, the inhibitory activity and mechanism of action of Auraplanin were estimated. CryoEM data collection was performed on a Titan Krios operated at 300 kV, equipped with a Falcon II direct electron detector.

Results: In this work, we have found a new inhibitor of protein synthesis, which binds in a completely new binding site. This compound is produced by *Actinoplanes sp.* VKM Ac-2862 and by Cryo-EM study of its complex with E.coli ribosome, it was shown, that it binds close to 560 loop of 30S ribosomal subunit. The new compound is a derivative of tetramic acid and we called it Auraplanin, because of bright orange color of the producer strain.

Structural data are in good agreement with genetic results – resistant mutations were located close determined binding site. Substitutions C564G, G558U, and G566A significantly increase minimal inhibitory concentration, all these mutations were not detected previously. We also observed resistant mutation in ribosomal protein S4, this mutation was previously identified as error-prone. Interestingly, ribosomal ambiguity mutations, G299A and G347U, also increased resistance to Auraplanin.

Conclusion: On the basis of the genetic, structural and biochemical studies we hypothesized that Auraplanin acts prevent the transfer from an open to a closed conformation of 30S subunit, in contrast to streptomycin, which promotes the formation of a closed state.

Key Words: cryo-ET

This work was supported by the Russian Foundation for Basic Research (Grant No. 19-34-51021)

*Corresponding author: Ilya Osterman. E-mail: i.osterman@skoltech.ru

OR-5

http://dx.doi.org/10.21103/IJBM.11.Suppl_1.OR5

Helicobacter pylori Surface Structures

Vladimir G. Zhukhovitsky, Tat'yana A. Smirnova,
Nataliya V. Shevlyagina

National Gamaleya National Research Centre for Epidemiology & Microbiology, Moscow, Russia

Background: *Helicobacter pylori*, which infects at least half of the human population, is an etiopathogenetic factor in the development of chronic gastritis (CG), gastric and duodenal ulcer disease (UD), and is also considered a risk factor in the occurrence of some forms of stomach cancer. Various surface structures of *H. pylori* are important pathogenic factors.

Methods: Reference (NCTC 11637, NCTC 11639) and freshly isolated *H. pylori* strains as well as samples of the gastric mucosa were examined using transmission (TEM) and scanning electron microscopy (SEM) by means of "JEM-100 B" (JEOL, Japan) and "Quanta 200 3D" (FEI Company, USA) systems, respectively. Samples for SEM fixed with formalin and not subjected to dehydration were sprayed with an electrically conductive layer of gold. Samples for TEM were prepared using negative contrast (NC) with ammonium molybdate and ultrathin sections (US) contrasted by Reynolds; fixation by Ito-Karnovsky was used in both cases. Accelerating voltage at TEM and SEM was 80 and 10 kV, respectively.

Results: Three types of *H. pylori* surface structures were found: flagella, fimbria, and vesicles. Flagella were found both in the material of cultures maintained in vitro and in each native sample of the gastric mucosa. SEM images suggest the involvement of flagella in biofilm formation. On longitudinal sections of the flagellum, the outer electron-dense layer and the inner content in the form of a filament were visualized; on cross sections, the flagellum looked like an annular structure with a centrally located point accumulation of electron-dense matter. Paradoxically, the *H. pylori* forms with a defective cell wall also possessed flagella. Freely located flagellar sheaths without central filament were often found in vitro only. Fimbriae were found exclusively in negatively contrasted pure bacterial cultures material. In addition, vesicles detaching from the surface of bacterial cells were found both in the material of aging *H. pylori* pure cultures and in native samples of the gastric mucosa under CG and UD. A small part of the vesicles retains their connection with the cell wall, while detached vesicles are present in excess in the surrounding space. Massive detachment of vesicles leads to the formation of spheroplasts, devoid of an outer membrane.

Conclusion: *H. pylori* has a representative set of surface structures that play an important role in the onset and development of the infectious process in the gastroduodenal area.

Key Words: *Helicobacter pylori*, flagella, fimbriae, vesicles

*Corresponding author: Vladimir G. Zhukhovitsky. E-mail: zhukhovitsky@rambler.ru

STRUCTURE OF VIRUSES AND CHAPERONINS

OR-6

http://dx.doi.org/10.21103/IJBM.11.Suppl_1.OR6

Baseplate Structure of Bacteriophage Phi812 and Mechanism of Cell Wall Binding and Penetration

Ján Biňovský¹, Marta Šiborová¹, Jiří Nováček¹, Mark Van Raaij²,
Pavel Plevka¹

¹Central European Institute of Technology, Masaryk University, Brno, Czech Republic

²Departamento de Estructura de Macromoléculas, Centro Nacional de Biotecnología (CSIC), Madrid, Spain

Background: Antibiotic-resistant strains of *Staphylococcus aureus* cause human infections that are difficult to treat and can lead to death. Bacteriophage (phage) phi812K1/420 from the family Myoviridae infects 95% of clinical isolates of *S. aureus* and therefore is a promising candidate for a phage therapy agent. As the native phage particle approaches its host cell, phage receptor-binding proteins make a contact with the host cell wall. This interaction triggers a cascade of structural changes in the baseplate resulting in phage tail contraction and genome ejection. Mechanistic description of the baseplate re-organization, however, remains unknown.

Methods: Using cryo-electron microscopy (cryo-EM), we studied the baseplate of the phage phi812K1/420. Also, selected proteins involved in the host cell wall binding and penetration were produced in recombinant form and their structures were solved using X-ray crystallography and cryo-EM single-particle reconstruction.

Results: We reconstructed the phage baseplate in native and contracted states. The reconstruction of the native baseplate reaches a resolution of 4 Å, which enables us to discern individual protein structures. Solved protein structures will be fitted into the reconstruction of the contracted baseplate.

Conclusion: Our results provide the first structural characterization of contractile phage infecting a Gram-positive bacterium. Comparison of the two distinct baseplate states will allow us to describe the molecular mechanism of the initial stage of phage infection in detail.

Key Words: *Staphylococcus aureus*, bacteriophage, cryo-EM

*Corresponding author: Ján Biňovský. E-mail: jan.binovsky@ceitec.muni.cz

OR-7

http://dx.doi.org/10.21103/IJBM.11.Suppl_1.OR7

Genome Release Mechanism of Picorna-Like Viruses

Pavel Plevka¹, Karel Škubník¹, Lukáš Sukeník^{1,2}, David Buchta¹,
Tibor Füzik¹, Antonín Přidal³, Robert Vácha^{1,2}

¹Central European Institute of Technology, Masaryk University, Brno, Czech Republic

²Department of Condensed Matter Physics and National Centre for Biomolecular Research, Faculty of Science, Masaryk University, Brno, Czech Republic

³Department of Zoology, Fishery, Hydrobiology, and Apidology, Faculty of Agronomy, Mendel University in Brno, Brno, Czech Republic

Protein capsids protect the genomes of viruses from degradation in the extracellular environment. However, virus capsids must release genomes into a host cell to initiate infection. We used cryo-electron microscopy to characterize

the genome release of viruses from the order Picornvirales: picornaviruses, dicistroviruses, and iflaviruses. These virus families include numerous human and animal pathogens. The viruses have non-enveloped virions and capsids organized with icosahedral symmetry. Their genome release can be induced in vitro by exposure to acidic pH, mimicking conditions in endosomes. We show that conformational changes of capsids and expansion of viral RNA genomes, which are induced by acidic pH, trigger the opening of picorna-like virus particles. The capsids of the studied viruses crack into pieces or open like flowers to release their genomes. The large openings of capsids enable the virus genomes to exit within microseconds, which limits the probability of their degradation by the RNases. Characterization of the virus genome release is the first step towards developing inhibitors of the process.

Key Words: cryo-EM, virus, genome, release.

***Corresponding author:** Pavel Plevka. E-mail: pavel.plevka@ceitec.muni.cz

OR-8

http://dx.doi.org/10.21103/IJBM.11.Suppl_1.OR8

Cryo-EM Structure of Mature Yellow Fever Virus

Valeriya R. Samygina^{1,2}, Eugeny B. Pichkur¹, Peter Cherepanov³, Alexey M. Egorov^{4,5}, Aydar A. Ishmukhametov^{4,6}, Michail F Vorovich^{4,6}

¹NRC "Kurchatov Institute," Moscow, Russia

²FRSC «Crystallography and photonics» RAS, Moscow, Russia

³The Francis Crick Institute, London, England

⁴FSBSI "Chumakov FSCR&DIBP" RAS, Moscow, Russia

⁵Faculty of Chemistry, M.V. Lomonosov Moscow State University, Moscow, Russia

⁶Sechenov First Moscow State Medical University, Moscow, Russia

Background: Yellow fever virus (YFV) is the prototype virus of the genus *Flavivirus*. It is endemic to sub-Saharan Africa and tropical South America. YF disease ranges from asymptomatic to severe jaundice and hemorrhagic fever. The flavivirus virion core is enveloped by a lipid membrane with integrated membrane (M) proteins and envelope (E) proteins that form the outer surface of the virion. The E protein provides stability to the viral particle and is responsible for early infection stages. Flaviviruses are heterogeneous in nature, which is related to their maturation process. Samples always contain mature, immature, half-mature, and damaged particles. Thus, cryo-EM is a method of choice for their structure determination. During the early stages of cryo-EM development, structures of flaviviruses were studied at 10–20 Å resolution. However, due to the progress of recent years, it became possible to determine flavivirus structures at a resolution of 5.6–2.6 Å. The cryo-EM method was used to obtain structural data of virions of dengue fever virus, Zika virus, TBE virus, etc. For YFV, only the cryo-EM structure of the immature virions at low resolution of 25 Å was determined (Y. Zhang et al. 2003 doi:10.1093/emboj/cdg270). However, the structure of mature (most infectious) YFV particles is still unknown.

Methods: Virus sample was produced in Vero cell culture. YFV-17D was inactivated and purified using ultracentrifugation. The concentration of viral particles in the target inactivated YFV-17D (iYFV-17D) was evaluated by spectrophotometry and by estimating the concentration of E protein determined by PAGE electrophoresis. Preliminary quality control of iYFV-17D sample was performed using negative staining TEM.

Cryo-EM data were collected using cryo-TEM Krios (Thermo-Fisher, USA) at 300kV using DED Falcon II. Dataset was preprocessed using Warp. Further processing was performed in Relion 3.1 and CisTEM. Model building was carried out using Isolve, Phenix and Coot software.

Results: A protocol of production and purification of highly concentrated (~2x10¹²) monodisperse inactivated iYFV-17D sample was developed. Cryo-EM structure of mature iYFV was solved at 4.1 Å resolution. The structure of YFV is similar to other known flavivirus structures, with 180 copies of protein E arranged in a herringbone pattern that makes up the icosahedral shell.

Conclusion: The high-resolution structure of mature iYFV-17D allowed to elucidate special features of this flavivirus and may be useful for vaccine improvement and drug development.

Key Words: flavivirus, cryoEM, structure

This work was supported by the Russian Foundation for Basic Research (Grant No. 18-02-40026)

***Corresponding author:** Valeriya Samygina. E-mail: lera@crys.ras.ru

OR-9

http://dx.doi.org/10.21103/IJBM.11.Suppl_1.OR9

Cryo-EM Structure of the Reconstituted Human γ -Tubulin Ring Complex

Marina Serna¹, Fabian Zimmermann², Artur Ezquerra¹, Rafael Fernandez-Leiro², Jens Luders², Oscar Llorca¹

¹Structural Biology Programme, Spanish National Cancer Research Centre (CNIO), Madrid, Spain

²Mechanisms of Disease Programme, Institute for Research in Biomedicine (IRB Barcelona), Barcelona, Spain

Background: Microtubules (MTs) are essential cytoskeletal polymers that provide structural support for the cell and play important roles in cell division, motility, and intracellular transport. The γ -tubulin ring complex (γ TuRC) is the major MT nucleator in animal cells. The molecular mechanism by which the γ TuRC promotes MT nucleation remains poorly understood although a template-based mechanism, remains the most widely accepted (Moritz et al., 2000, Kollman et al., 2010). According to this model γ TuRC, a 2 MDa multi-subunit protein complex, forms a lock washer-like structure, in which γ -tubulin molecules are arranged in a ring-shaped structure that serves as a template for the assembly of $\alpha\beta$ -tubulin heterodimers.

Methods: We have set up an in vitro system to purify the human γ TuRC using infected insect cells with recombinant baculoviruses. This complex sample was subjected to cryo-EM analysis and single-particle reconstruction.

Results: We have demonstrated that RUVBL1-RUVBL2 AAA-ATPase complex (RUVBL) controls the assembly and composition of γ TuRC in human cells both in vivo and in vitro. Likewise, RUVBL assembles γ TuRC from a minimal set of core subunits in a heterologous co-expression system. Purified, reconstituted γ TuRC has nucleation activity and resembles native γ TuRC (Consolati et al., 2020, Liu et al., 2020, Wiczorek et al., 2020), as revealed by its cryo-EM structure at ~4.0 Å resolution.

Conclusion: We have been able to identify novel mechanistic and structural features that determine the intricate, higher-order γ TuRC architecture (Zimmermann, Serna et al., 2020).

Key Words: Cryo-EM, RUVBL, γ TuRC, microtubules

***Corresponding author:** Marina Serna. E-mail: mserna@cnio.es

ADVANCES IN EM TECHNOLOGY AND PROCESSING

P-1

http://dx.doi.org/10.21103/IJBM.11.Suppl_1.P1**Analysis of Tick-borne Encephalitis Virus Single-particle Imaging on X-ray Free-electron Laser**Grigoriy A. Armeev¹, Alexey K. Shaytan¹, Mikhail F. Vorovich², Alexey M. Egorov², Aydar A. Ishmukhametov², Mikhail P. Kirpichnikov¹, Konstantin V. Shaitan¹¹Department of Biology, Lomonosov Moscow State University, Moscow, Russia²FSAS "Chumakov FSC R&D IBP RAS" (Institute of Poliomyelitis), Moscow, Russia

Background: Tick-borne encephalitis virus (TBEV) is a dangerous human pathogen which envelope structure is already known from cryoEM study. TBEV mature viral particle size (~50 nm in diameter) makes it suitable for single-particle imaging (SPI) on X-ray free-electron laser (XFEL). XFEL SPI studies are at the early stages of development; thus, a well-described and conformationally homogeneous sample is required to develop approaches for experimental setup and data analysis. Here we present the image analysis results of data collected in October 2019 during the European XFEL experiment #2316.

Methods: The detector was placed at 1.62 m from the injector; photon energy was around 6 keV, pulse energy 4 mJ, beam diameter ~ 500 nm. All runs were processed to detect hits with threshold filter (5th percentile of lit pixels) and further filtered to omit low-intensity images and images that lack detector modules. Filtered hits were background and geometry corrected with SPImage library and custom python scripts. Then hits were azimuthally integrated using PyFAI library. Scattering profiles were further clustered using the affinity propagation algorithm with cosine similarity metric in log space. Extracted classes were used to build averaged images. All hit profiles were fitted with model scattering to estimate the diameter of the particle. Simulated diffraction patterns were prepared using Condor from the cryoEM electron density map (EMDB ID 3752).

Results: During the analysis after the filtering, only 276 clean and bright hits were collected per 135 min of injection (from 27287 hits detected via lit pixels threshold). Thus the hit rate was around ~ 2 hits/min, which is expected to rise in the future. The majority of hits correspond to the 40-50 nm particles (Fig. 1a), which is expected for TBEV. However, the exact size may vary due to solvent evaporation, ion condensation, and possible variability in the sample.

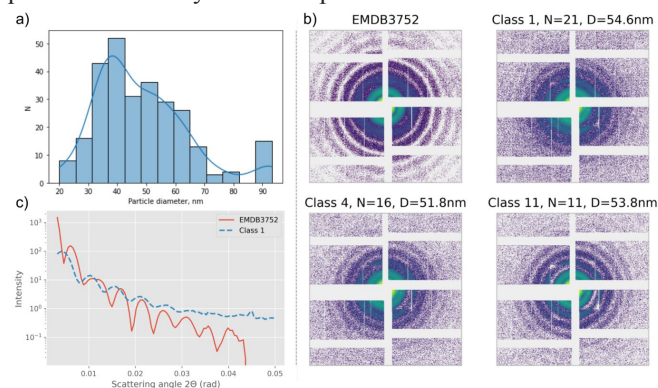


Fig. 1. a) Particles size distribution. b) Comparison of averaged images with modeled diffraction. c) Comparison of scattering profiles of averaged class 1 with diffraction modeled from cryoEM density map.

Conclusion: The averaged images and their scattering profiles correlate with the simulated scattering patterns, though not ideally (Fig. 1 bc). Such discrepancy is expected due to the absence of electron density in the center of modeled viral structures.

Key Words: XFEL, single-particle imaging, viruses

This work was supported by the Russian Foundation for Basic Research (Grants No. 18-02-40010 (data analysis) and 18-02-40026 (sample preparation)).

*Corresponding author: Grigoriy Armeev. E-mail: armeev@intbio.org

P-2

http://dx.doi.org/10.21103/IJBM.11.Suppl_1.P2**Multiscale Molecular Dynamics Simulations of the Skin Membranes as a Tool for the Interpretation of the Transmission Electron Microscopy Images**

Marine E. Bozdaganyan

Biological Faculty, Lomonosov Moscow State University, Moscow, Russia

Background: Human skin can inhibit chemical penetration which limits the clinical applications of transdermal drug delivery. The stratum corneum (SC) is the primary barrier and organized in lamellar membranes containing the lipids of ceramides (CER), free fatty acids (FFA), and cholesterol (CHOL). One of the most widely used ways to overcome the SC is the addition of chemical penetration enhancers (CPEs) to active ingredients. There are various methods, which have been employed to explore the mechanisms by which CPEs with drugs can change the morphology of SC including transmission electron microscopy. Here, we propose to use multiscale coarse-grained (CG) molecular dynamics (MD) simulations for the interpretation of the images of the SC from the electron microscopy experiments.

Method: We utilized the MARTINI force field for the CG simulations. We employed the mixed-lipid bilayer model of SC consisting of CER, CHOL, and FFA in a 1:1:1 molar ratio assembled with CHARMM-GUI web-service. The systems of the SC model membrane and various enhancers were simulated in the NPT ensemble with the polarizable water model and the reaction field approach for the long-range electrostatics with the usage of Gromacs 2019.4 software.

Results: The membrane model was validated with standard characteristics: thickness, diffusion of the lipids, order parameters, and density profiles. After, we have added CPEs and active ingredients to the systems: menthol and osthole as control simulations, ethanol with linoleic acid and lidocaine as test simulations. We have observed the membrane desegregation in the case of menthol and osthole formulations similar to the published results while the permeation of lidocaine with ethanol and linoleic acid did not cause the disruption of the membranes but increased its fluidity and permeability properties.

Conclusion: The method of multiscale coarse-grained molecular dynamics simulations can be utilized for the prediction and interpretation of morphology change of SC in addition to various substances.

Key Words: chemical penetration enhancers; stratum corneum; multiscale molecular dynamics simulations; TEM imaging

This research was funded by the Russian Science Foundation (Grant 19-71-00109)

P-3

http://dx.doi.org/10.21103/IJBM.11.Suppl_1.P3

The Structure of Self-Assembled Surfactant Micellar Networks by *in situ* Cryo-Electron Tomography

Yury M. Chesnokov¹, Andrey V. Shibaev³, Roman A. Kamyshinsky^{1,2}, Vyacheslav A. Kralin², Olga E. Philippova³, Anton S. Orekhov^{1,2}

¹National Research Centre "Kurchatov Institute," Moscow, Russia

²Moscow Institute of Physics and Technology, Moscow, Russia

³Department of Physics, Lomonosov Moscow State University, Moscow, Russia

Background: Surfactant molecules can form various self-assembled structures in aqueous solutions, including spherical and cylindrical micelles, lamellae, vesicles, etc. Elongated cylindrical (wormlike) micelles can entangle and form a dense network. The study of the un-perturbed native structure of wormlike micelles in such networks presents a great challenge, since the micelles are formed due to weak non-covalent interactions and may easily break when external conditions are changed. In this work *in situ* cryo-electron tomography (cryo-ET) was applied to reveal the relaxed structure of such entangled systems.

Methods: To prepare samples for the cryo-ET study 1 μ l of the aqueous surfactant-containing solution was applied to the glow discharged grid, blotted with filter paper for 10 sec, drained for 60 sec to allow for the relaxation of the system and plunge-frozen with Vitrobot Mark IV. The vitrified sample was transferred to Versa 3D cryo-focused ion beam / scanning electron microscope (cryo-FIB/SEM) to prepare thin (100-150 nm) sections of the sample. Cryo-ET study was conducted using Titan Krios. IMOD and Avizo software packages were used for data processing.

Results: In this work, wormlike micelles formed by a mixture of an anionic and a cationic surfactant were investigated at the excess of the anionic surfactant. Cryo-ET study of the obtained lamellae demonstrated the formation of two different phases, consisting of straight rods oriented along the grid substrate (phase 1) and isotropic network formed by wormlike micelles (phase 2) above it. The topology of the second phase corresponded to the branched saturated network or entangled network depending on cation/anion ratio of the sample. However, the analysis of the thin samples obtained without cryo-FIB demonstrated only the presence of the metastable phase (phase 1), which could lead to false conclusions regarding the morphology of the micelles.

Conclusion: Here we discuss the influence of different sample preparation approaches on the sample structure and demonstrate that the native un-perturbed conformation of charged cylindrical surfactant micelles in the dense network is that of a slightly bent rod or a wormlike chain with high persistence length.

Key Words: cryo-electron tomography, cryo-FIB, surfactants, wormlike micelles

This work was financially supported by the National Research Center "Kurchatov Institute" (order dated 02.07.2020 No. 1056).

***Corresponding author:** Yury Chesnokov. E-mail: chessyura@yandex.ru

P-4

http://dx.doi.org/10.21103/IJBM.11.Suppl_1.P4

Robust Method for Background Subtraction in Serial X-ray Diffraction Data

Egor Marin², Daniil Vakhrameev¹, Anastasiia Gusach¹, Aleksandra Luginina¹, Kirill Kovalev^{1,3}, Wei Liu⁴, Uwe Weierstall⁴, Jaehun Park², Ki Hyun Nam², Cho Yunje², Alexey Mishin¹, Vadim Cherezov^{1,5}, Valentin Borshchevskiy¹

¹Research Center for Molecular Mechanisms of Aging and Age-related Diseases, Moscow Institute of Physics and Technology, Dolgoprudny, Russia

²Pohang Accelerator Laboratory, POSTECH, Pohang, Republic of Korea

³Forschungszentrum Julich, Julich, Germany

⁴School of Molecular Sciences and Biodesign Center for Applied Structural Discovery, Biodesign Institute, Arizona State University, Tempe, Arizona, USA

⁵Bridge Institute, Department of Chemistry, University of Southern California, Los Angeles, California, USA

Background: Membrane receptors play an important role in signal transduction across the cell membrane in all living organisms. Their structural studies have been enabled by multiple technological breakthroughs in their heterologous expression, stabilization, crystallization, and crystallographic data collection as well as in cryogenic electron microscopy (cryoEM). During the last decade, serial femtosecond crystallography (SFX) using X-ray free-electron lasers (XFELs) has enabled structure determination of previously inaccessible proteins, including several G-protein-coupled receptors (GPCR), that produce only micrometer-sized crystals, thus paving the way towards understanding their activation mechanism and rational drug discovery. In addition to experimental difficulties, membrane protein structure determination is also often accompanied by data processing challenges. In particular, the lipidic cubic phase that serves as a carrier for membrane protein microcrystals, as well as various XFEL beam-shaping devices may generate substantial background scattering that could complicate the structure factor extraction from the diffraction images.

Methods: In this work, we tested an adaptation of the denoising algorithm via matrix decomposition to XFEL-SFX data. We benchmarked its performance using high-background data from PAL-XFEL and established its applicability to serial crystallography image denoising, as well as compared it to the CrystFEL-based image denoising algorithm.

Results: We find that, although the decomposition-based image denoising does not outperform CrystFEL median subtraction, it performs better than the integration without any additional subtraction. We find the non-negative matrix factorization performing better than more traditional singular-value decomposition methods, both in terms of visual interpretability and final data quality.

Conclusion: We hope that this work will draw attention to background subtraction methods in structural biology, and will pave the way towards the processing of the most challenging datasets in structural biology, particularly, those collected from membrane proteins.

Key Words: serial crystallography, background subtraction, membrane proteins.

This work was by the Ministry of Science and Higher Education of the Russian Federation (agreement #075-00337-20-03, project FSMG-2020-0003)

***Corresponding author:** Egor Marin. E-mail: marin@phystech.edu

P-5

http://dx.doi.org/10.21103/IJBM.11.Suppl_1.P5

Functional and Structural Studies on Human ASCT2 Transporter — A Promising Drug Target

Valery Novoseletsky, Mikhail Lozhnikov, Grigoriy Armeev, Aleksandr Kudriavtsev, Alexey Shaytan, Georgiy Kobelkov, Konstantin Shaitan

M. V. Lomonosov Moscow State University, Moscow, Russia

Background: Protein structure determination using X-ray free-electron laser (XFEL) includes analysis and merging a large number of snapshot diffraction patterns. Convolutional neural networks are widely used to solve numerous computer vision problems, e.g. image classification, and can be used for diffraction pattern analysis. But the task of protein structure determination with the use of CNNs only is not yet solved.

Methods: We simulated the diffraction patterns using the Condor software library and obtained more than 1000 diffraction patterns for each structure with simulation parameters resembling real ones. To classify diffraction patterns, we tried two approaches, which are widely known in the area of image classification: a classic VGG network and residual networks.

Results: 1. Recognition of a protein class (GPCRs vs globins). Globins and GPCR-like proteins are typical α -helical proteins. Each of these protein families has a large number of representatives (including those with known structure) but we used only 8 structures from every family. 12,000 of diffraction patterns were used for training and 4,000 patterns for testing. Results indicate that all considered networks are able to recognize the protein family type with high accuracy. 2. Recognition of the number of protein molecules in the liposome. We considered the usage of liposomes as carriers of membrane or globular proteins for sample delivery in XFEL experiments in order to improve the X-ray beam hit rate. Three sets of diffractograms for liposomes of various radius were calculated, including diffractograms for empty liposomes, liposomes loaded with 5 bacteriorhodopsin molecules, and liposomes loaded with 10 bacteriorhodopsin molecules. The training set consisted of 23625 diffraction patterns, and test set of 7875 patterns. We found that all networks used in our study were able to identify the number of protein molecules in liposomes independent of the liposome radius. Our findings make this approach rather promising for the usage of liposomes as protein carriers in XFEL experiments.

Conclusion: Thus, the performed numerical experiments show that the use of neural network algorithms for the recognition of diffraction images from single macromolecular particles makes it possible to determine changes in the structure at the angstrom scale.

Key Words: X-ray crystallography, diffraction pattern, protein structure, neural networks.

This work was supported by the Russian Foundation for Basic Research (Grant No. 18-02-40010)

***Corresponding author:** Valery Novoseletsky. E-mail: valery.novoseletsky@yandex.ru

P-6

http://dx.doi.org/10.21103/IJBM.11.Suppl_1.P6

Automated Pipeline for Parametrization of the Coarse-Grained Models for Biomolecular Simulations

Philipp S. Orekhov

Faculty of Biology, Lomonosov Moscow State University, Moscow, Russia

Background: Despite the advances in computational techniques and computing resources, the atomistic simulations are still limited in terms of attainable simulation time (up to 1-100 μ s) and system size (up to millions of atoms). Various coarse-grained models provide a valuable alternative to the fully atomic simulations but they largely rely upon the rigorous parametrization procedure. The latter is required to obtain a set of coarse-grained force field parameters adequately reproducing the behavior of the original full-atom system.

Here, we report an automated pipeline designed for the parametrization of coarse-grained models of small organic compounds and polymers. While it is tailored to the MARTINI coarse-graining framework, it can also be applied to other force fields following a similar coarse-graining strategy.

Methods: Given the all-atom trajectory and the mapping (i.e., a table describing the correspondence between atoms and coarse-grained particles), the parametrization procedure iteratively optimizes bonded parameters of the coarse-grained model such that the bond, angle, (if required) dihedral histograms obtained from a series of coarse-grained simulations gradually converge to the target distributions derived from the full-atom trajectory mapped to the CG resolution.

Results: The developed pipeline accepts as an input a full-atom trajectory of a molecule to be parametrized as well as the mapping between the full-atom and coarse-grained models. Based on this input, the initial coarse-grained model is built using Boltzmann inversion, which is a subject for the following iterative optimization. At each iteration, the convergence of bonded terms is checked based on the overlap of respective histograms derived from full-atom and coarse-grained simulations and, in case of satisfactory convergence, the optimization is stopped. In addition to the parametrization of individual compounds, the pipeline also allows deriving models for polymers consisting of repetitive units.

The proposed here approach has been successfully used to create coarse-grained topologies for various small molecular weight compounds, such as drugs and antiseptics, as well as for detergents (DDM) and amphiphilic polymers (SMA, DIBMA) stabilizing lipodiscs – nanosized lipid particles widely exploited in structural studies of membrane proteins. The later models proved themselves particularly helpful for the interpretation of experimental data from small-angle scattering, EM, and EPR experiments

Conclusion: We expect that the developed pipeline would support the fast and straightforward development of coarse-grained models for simulations of biomolecular systems and new materials. Such simulations can be especially useful for the interpretation of experimental data obtained by, e.g., small-angle scattering and Cryo-EM experiments.

The pipeline is available online at <https://github.com/porekhov/cgmktop>.

Key Words: molecular dynamics, coarse-grained models

This work was supported by the Russian Science Foundation (Grant No. 19-74-00065)

***Corresponding author:** Philipp Orekhov. E-mail: orekhov@mail.bio.msu.ru

P-7

http://dx.doi.org/10.21103/IJBM.11.Suppl_1.P7

NdFeCo-based Nanoparticles for Biomedical Applications

Vadim Yu. Samardak, S.A. Azon, Aleksei Yu. Samardak, Evgeniy K. Papyrov, Alexander S. Samardak, Aleksei V. Ognev

Laboratory of Thin Film Technologies, School of Natural Sciences, Far Eastern Federal University, Vladivostok, Russia

Background: The multifunctional nanoparticles can be promising antitumor materials. The results of a study of synthesized NdFeCoB oxide nanoparticles (NPs) as a basis for drug transportation systems are presented. In the next step, the NPs can be coated by a multifunctional gel shell.

Methods: NPs, the composition of NdFexCo1-xB (where x = 0, 0.05, 0.1, 0.2, 0.3, 0.4, and 0.5), were synthesized by a Pechini-type sol-gel method. The synthesis allows tuning of NPs magnet properties by manipulating the microstructure and phase composition. NPs were studied by XRD, SEM, TEM, HRTEM, and VSM.

Results: SEM images show that the average size of NPs changed from 280 nm (for x = 0) up to 416 nm (for x = 0.1 – 0.5). At TEM images the NPs of the sample without cobalt (x = 0) have an elongated shape (Fig 1a). Diffraction patterns showed that the NPs consist of single crystal or ordered crystallites. NPs with cobalt mainly consist of crystallites with a size of about 20-50 nm. There are also areas with a complex-grained microstructure. Hysteresis loops and first-order reversal curve analysis indicated that the NPs were ferromagnetic whose coercivity, squareness ratio, and magnetic interactions changed significantly with the cobalt contents.

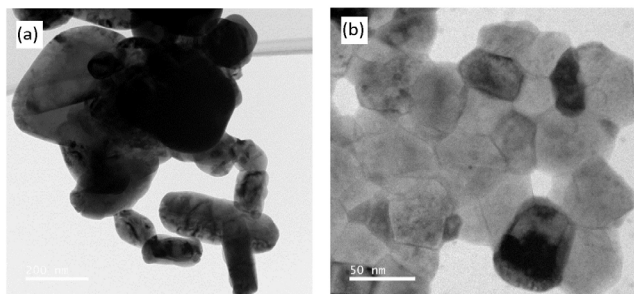


Fig. 1. TEM images of NdFe_{1-x}Co_xB oxide particles with x=0 (a) and 0.5 (b)

Conclusion: The features of the crystal structure and magnetic properties of the synthesized NdFeCoB oxide NPs depending on the concentration of cobalt have been established.

Key Words: magnetic nanoparticles, biomedicine, crystal structure

The research was carried out with the support of the Russian Science Foundation (project 19-72-20071)

*Corresponding author: Vadim Samardak. E-mail: samardak_vy@dfvu.ru

P-8

http://dx.doi.org/10.21103/IJBM.11.Suppl_1.P8

Fe₂O₃-SiO₂-Au Core-Shell Nanoparticles for Theranostics

Vadim Yu. Samardak¹, Mukhamad Sobirov¹, Aleksei V. Ognev¹, Alexander S. Samardak¹, Thomas M. Koo², Young K. Kim²

¹Laboratory of Thin Film Technologies, School of Natural Sciences, Far Eastern Federal University, Vladivostok, Russia

²Department of Materials Science & Engineering, Korea University, Seoul, Republic of Korea

Background: Core-shell nanoparticles (NPs) Fe₃O₄-SiO₂ covered with Au grains due to their unique magnetic, biological, optical and mechanical properties are promising nanostructured material especially in biomedical field. Magnetic core allows controlling the position of NPs, SiO₂ shell makes them biocompatible and decrease magnetostatic interactions between them, and Au NPs on the surface allow creating additional matrix around them and using such systems as controlled nanocontainers in tasks of drug delivery, magnetic resonance imaging and target cancer cell therapy.

Methods: Inner magnetic core of the NPs was synthesized using polyol method, a 3-step process which resulting in magnetite NPs with hydrophilic surface. Shell was made by covering Fe₃O₄ particles in surfactant and growing SiO₂ on top of them by sol-gel method. Covering core-shell NPs with 3.5 nm Au seed grains using monosilane and their further growth to control diameter. Structural properties were studied using TEM and Dual Beam SEM. Magnetic properties were investigated using LakeShore VSM 7400 magnetometer.

Results: Two samples with different concentration of Au NPs were investigated. SEM observations show that core-shell Fe₃O₄-SiO₂ are spherical with average diameter of 200 nm and Au NPs with diameter of 15 nm are evenly dispersed on their surface. Magnetic measurements showed that different concentration of Au NPs results in different coercive forces of the sample. Decreasing the temperature to 77 K showed up to 6 times increase of coercive force and slight increase in magnetization.

Conclusion: Biocompatible magnetic nanoparticles are critical advances in biomedical applications. In this work, we studied the morphology of the samples, demonstrated the change of coercive force of NPs with different Au concentration and investigated their magnetic properties in low temperatures.

Key Words: magnetic nanoparticles, biomedicine, low temperature, cancer cell therapy

Authors would like thank the support of the Russian Ministry of Science and Higher Education under the state task (0657-2020-0013)

*Corresponding author: Aleksei Samardak. E-mail: samardak. aiu@dfvu.ru

P-9

http://dx.doi.org/10.21103/IJBM.11.Suppl_1.P9

Excess of Nhp6 over Spt16/Pob3 is Necessary for Efficient Nucleosome Unfolding by yFACT

Anastasiia L. Sivkina¹, Daria K. Malinina¹, Alexey V. Feofanov^{1,2}, Vasily M. Studitsky^{1,3}

¹Biology Faculty, Lomonosov Moscow State University, Moscow, Russia

²Institute of Bioorganic Chemistry, Moscow, Russia

³Fox Chase Cancer Center, Philadelphia, Pennsylvania, USA

Background: DNA accessibility in chromatin is important for proper gene expression and is regulated by multiple factors. One of them is histone chaperone FACT, which conducts large-scale ATP-independent nucleosome unfolding

that increases the accessibility of nucleosomal DNA. FACT binding results in dramatic DNA uncoiling from nucleosome, occurs without apparent loss of histones, and proceeds via an 'all-or-none' mechanism, but the detailed mechanism of this process is still unknown. FACT-dependent nucleosome unfolding modulates the accessibility of nucleosomal DNA, and it is an important function of FACT in the processes of transcription, DNA replication, and repair *in vivo*.

Methods: Nucleosome-positioning DNA sequences containing fluorescent labels (Cy3 and Cy5) at positions 13/91 or 35/112 from the nucleosome boundary were used. Nucleosomes were assembled by transfer of histone octamers from chicken chromatin to nucleosomal DNA during dialysis from 2M NaCl. After dialysis nucleosomes were gel purified and used at a final concentration of 0.5nM for spFRET measurements or at 10nM for EMSA analysis. For complex formation nucleosomes were incubated in the presence of Spt16/Pob3(0.13 μ M) and Nhp6(1.3 μ M) for 10 min at 30°C in buffer containing 17mM HEPES, 2mM Tris-HCl, 0.8mM Na3EDTA, 0.11mM 2-mercaptoethanol, 150mM KCl, 11mM NaCl, 1.1%glycerin, 12% sucrose.

In spFRET microscopy analysis, the proximity ratio EPR from each nucleosome was calculated based on the intensity of the signals, corrected to the background and plotted as relative frequency distribution. Each plot was fitted as a sum of two Gaussians to describe two conformational states of nucleosomes. The fractions of nucleosomes in different states were estimated by calculating the surface of areas under the corresponding Gaussian peaks as a fraction of the total area of the plot.

Results: Here we report the results of our analysis of nucleosome unfolding by yeast FACT (yFACT) at different ratios of Spt16/Pob3 and Nhp6 using single-particle Förster resonance energy transfer (spFRET) microscopy. Our analysis suggests that the optimal ratio of Spt16/Pob3 to Nhp6 for the most efficient FACT-dependent nucleosome unfolding is 1:10. Importantly, a mere increase in the concentration of FACT results in a decrease of the functional activity, suggesting that the formation of a functional complex having a certain stoichiometry of Spt16/Pob3 to Nhp6 is essential for efficient FACT-dependent nucleosome unfolding.

Conclusion: We determined that a certain ratio of Spt16/Pob3 to Nhp6 is essential for efficient FACT-dependent nucleosome unfolding, suggesting the formation of a functional FACT: Nhp6 complex.

Key Words: chromatin, FACT, nucleosome, remodeler

This work was supported by the Russian Science Foundation (Grant No. 19-44-02013)

***Corresponding author:** Anastasiia Sivkina. E-mail: anastasiia.sivkina@gmail.ru

STRUCTURE OF MEMBRANE PROTEINS

P-10

http://dx.doi.org/10.21103/IJBM.11.Suppl_1.P10

Solvatochromic Fluorescent Dyes Tested for Spectroscopic Measurements of Protein Conformational Dynamics

Anatoly Belousov¹, Ivan Maslov¹, Polina Khorn¹, Alexander Mishin², Mikhail Baranov², Thomas Gensch³, Valentin Borshchevskiy^{1,3}

¹Moscow Institute of Physics and Technology, Dolgoprudny, Russia

²Shemyakin-Ovchinnikov Institute of Bioorganic Chemistry, Russian Academy of Sciences, Moscow, Russia

³Forschungszentrum Jülich, Jülich, Germany

Background: Recoverin is a 23 kDa protein, belonging to the superfamily of EF-hand Ca²⁺-binding proteins. One of the functions of recoverin is to regulate the activity of the rhodopsin kinase GRK1, which regulates the activity of rhodopsin. In dim ambient light, the level of calcium in the rod cells of the retina is high, so recoverin binds to and inhibits rhodopsin kinase, leaving rhodopsin very sensitive to photons to enable the eye to detect visual signals even under low-light conditions. Many biophysical methods have previously been used to study the conformational dynamics of recoverin, including NMR, SPR and fluorescence spectroscopy. Here we describe fluorescent solvatochromic dyes suitable for spectroscopic observation of conformational changes in recoverin.

Methods: We tested four fluorescent dyes, which were covalently attached to Cys39 of recoverin via the thiol-maleimide interaction.

Results: Two out of four labeled recoverin samples showed EGTA-induced changes in the fluorescence lifetime and excitation and emission spectra.

Conclusion: Our experiments show solvatochromic fluorescent dyes that can be successfully used for spectroscopic observation of conformational dynamics in proteins.

Key Words: EF-hand protein, spectroscopy, fluorescent solvatochromic dyes

This work was supported by the Russian Foundation for Basic Research (Grant No. 20-34-70034)

***Corresponding author:** Anatoly Belousov. E-mail: belousov.as@phystech.edu

P-11

http://dx.doi.org/10.21103/IJBM.11.Suppl_1.P11

Microscale Thermophoresis of Mycobacterial Cytochrome P450 with Azole Drugs

Ivan Kapranov¹, S. Bukhdruker¹, M. Karpova², Yulia Zagryadskaya¹, Ivan Okhrimenko¹, A. Gilep³, N. Strushkevich², Valentin Borshchevskiy¹

¹Moscow Institute of Physics and Technology (National Research University), Moscow, Russia

²Skolkovo Institute of Science and Technology, Moscow, Russia

³Institute of Bioorganic Chemistry of NASB, Moscow, Russia

⁴ESRF – The European Synchrotron, Grenoble, France

Background: Cytochrome P450 family members are found in most organisms where they are involved in the metabolism and synthesis of steroids, bile acids, unsaturated fatty acids, phenolic metabolites as well as exogenic chemicals. Drugs targeting cytochrome P450 have been shown to inhibit the growth of *Mycobacterium tuberculosis*, the causative agent of one of the deadliest diseases – tuberculosis. Recently, we showed that CYP124, CYP125, and CYP142 can bind and metabolize a panel of human immunoactive oxysterols *in vitro* (Varaksa et al., 2021) and one of them (CYP124) can metabolize antituberculosis drugs (Bukhdruker et al., 2020). Thus, inhibition of cytochrome P450 is a promising strategy for the development of new anti-tubercular drugs.

The existing methods used to assess protein-ligand interactions for cytochromes P450 (spectral titration and Surface Plasmon Resonance) have a number of limitations. In

this regard, we used an alternative approach for this purposes – microscale thermophoresis (MST) which was not previously used for proteins of the cytochrome P450 superfamily

Methods: Here we show that MST can be used to determine the micromolar-range dissociation constants (Kd) of membrane-associated mycobacterial cytochrome CYP124 with small-molecule azole drugs. CYP124 was fluorescently labeled with Cy3-NHS and MST curves were collected at Monolith NT.115 instrument (blue/green channel, NanoTemper Technologies) in presence of various concentrations of azole compounds: econazole, ketoconazole, itraconazole, and miconazole. The experimental results were approximated by the second-order bimolecular binding equation as well as by the Hill-Langmuir equation.

Results: Therefore, MST is a valuable method for the assessment of cytochrome P450 binding to their ligands for cases when traditional approaches are not applicable. The binding regime of CYP124 with azole derivatives was characterized by the structure of the CYP124 complex with carboxyhexyl imidazole solved with ~1 Å resolution.

Conclusion: We have developed a set of techniques for chromatin modeling on the nucleosomal level. Such approaches tightly integrate various experimental data (mainly corrected spFRET efficiencies and hydroxyl DNA footprints) into molecular modeling pipelines.

Key Words: tuberculosis, cytochrome P450, microscaled thermophoresis.

This work was supported by a joint grant of Belarusian Republican Foundation for Fundamental Research, B20R-061 and Russian Foundation for Basic Research, 20-54-00005

***Corresponding author:** Ivan Kapranov. E-mail: kapranov.ia@phystech.edu

P-12

http://dx.doi.org/10.21103/IJBM.11.Suppl_1.P12

Three-dimensional Structure of the Yeast Transmembrane Mechanosensor Wsc1

Maria Karlova¹, Natalia Voskoboinikova², Armen Y. Mulikjanian^{2,3}, Konstantin V. Shaitan¹, Heinz-Jürgen Steinhoff², Jürgen J. Heinisch⁴, Olga S. Sokolova¹

¹Department of Bioengineering, Faculty of Biology,

M. V. Lomonosov Moscow State University, Moscow, Russia

²University of Osnabrück, Faculty of Physics, Osnabrück, Germany

³Faculty of Bioengineering and Bioinformatics and Belozersky Institute of Physico-Chemical Biology, M. V. Lomonosov Moscow State University, Moscow, Russia

⁴University of Osnabrück, Faculty of Biology/Chemistry, Department of Genetics, Osnabrück, Germany

Background: Wsc1 is the best studied of the five mechanosensors of the cell wall integrity (CWI) signal transduction pathway in *Saccharomyces cerevisiae*. In genetic and biophysical studies, Wsc1 functions were assessed either in living yeast cells or in crude cell extracts. So far, no attempts to purify the sensor and determine its structure have been reported.

Methods: The Wsc1-green fluorescent protein (GFP) fusion was expressed in *S. cerevisiae* following standard protocols. For solubilization, a 5% (w/v) solution of styrene-maleic acid (SMA) copolymer was added dropwise to the membrane suspension to get a final cell-to-SMA weight ratio of 1:2.5. The suspension

was incubated for 30 min at room temperature (RT) and then for 16 hours at 4 °C, followed by centrifugation for 20 min at 134000 g at 4 °C. The supernatant was subsequently purified on affinity resin. Protein samples (3 µL) were placed onto the glow-discharged grid, stained twice, using 1% aquatic uranyl acetate solution for 30 s at RT, and air-dried. Micrographs were acquired using a transmission electron microscope Jem-2100 (Jeol, Japan) equipped with a 2K x 2K CCD camera Ultrascan 1000XP (Gatan, USA). The microscope operated at 200 kV in a low dose mode, with a magnification x40000 (2.5 Å/pix) and defocus 0.5-1.9 µm. Images were acquired automatically with SerialEM software.

Results: We applied the 3:1 SMA copolymer to isolate Wsc1-GFP fusions into SMA/lipid particles (SMALPs) directly from native yeast membranes. We purified Wsc1-GFP-containing SMALPs by affinity chromatography; characterization by dynamic light scattering confirmed the presence of monodisperse nano-sized particles. The intensity-weighted diameter was estimated to be in the 10-nm range. The purified Wsc1-GFP-containing SMALPs were further analyzed by transmission electron microscopy (TEM). 46500 single particles were used to generate the 3D reconstructions of Wsc1-GFP. The resulting model showed the three functional parts of the Wsc1 sensor: the extracellular part, which has a clasp-like appearance, the transmembrane domain, and the short cytosolic part of Wsc1 fused to the GFP beta-barrel.

Conclusion: The 3:1 SMA copolymer enabled isolation of Wsc1-GFP fusion complexes into SMALPs directly from native yeast membranes. Image analysis of the TEM data showed the Wsc1 in its contracted conformation. We propose a model of conformational changes in Wsc1 in response to mechanical stress.

Key Words: Wsc1, detergent-free extraction, SMA copolymer, membrane protein, transmission electron microscopy, 3D reconstruction

This work was funded jointly by German Research Foundation (DFG, STE640/15) to H.J.S., and RFBR grant no. 18-504-12045 to K.V.S

***Corresponding author:** Maria Karlova. E-mail: mkarlova@yandex.ru

P-13

http://dx.doi.org/10.21103/IJBM.11.Suppl_1.P13

Structural Studies of Insulin Receptor-Related Receptor Ectodomain

Andrey Mozhaev^{1,2}, Evgeny Pichkur³, Igor Deyev¹, Ekaterina Mileschina¹, Anton Orekhov³, Alexander Vasiliev^{2,3}, Alexander Petrenko¹

¹Shemyakin-Ovchinnikov Institute of Bioorganic Chemistry RAS, Moscow, Russia

²Shubnikov Institute of Crystallography of FRSC "Crystallography and Photonics" RAS, Moscow, Russia

³National Research Center "Kurchatov Institute," Moscow, Russia

Background: The insulin receptor-related receptor (IRR) was originally discovered due to its high homology to the other family members (insulin receptor and insulin-like growth factor 1 receptor). We determined that IRR can be activated by mildly alkaline extracellular media and has typical features of the ligand-receptor interaction, including its specificity and

dose-dependence. Since pH-sensitive properties of IRR are determined by its ectodomain; therefore, we chose as an option to study the soluble extracellular domain IRR.

Methods: The investigation carried out in Titan Krios 60-300 TEM/STEM (FEI, USA) CryoEM, equipped with direct electron detector Falcon II (FEI, USA) and Cs image corrector (CEOS, Germany), at an accelerating voltage of 300 kV. Data processing and 3D reconstruction were carried out using computing resources of the Federal Collective Usage Center Complex for Simulation and Data Processing for Mega-Science Facilities at NRC "Kurchatov Institute."

Results: The obtained 2D classifications of particles of the ectodomain IRR at a neutral pH form several 3D models. This indicates that the ectodomain has several possible conformations, which is consistent with our previously obtained data using SEC-SAXS and AFM. In the future, additional careful data processing is required, as well as studies of the IRR ectodomain in mildly alkaline pH.

Conclusion: In this study, we presented the structural characteristics of the IRR ectodomain obtained by CryoEM. These results are an important step towards understanding the mechanism of functioning of the IRR.

Key Words: receptor tyrosine kinases, insulin receptor-related receptor (IRR), CryoEM

This work was supported by the Russian Foundation for Basic Research (Grant No. 20-04-00959)

***Corresponding author:** Andrey Mozhaev. E-mail: a.a.mozhaev@gmail.com

P-14

http://dx.doi.org/10.21103/IJBM.11.Suppl_1.P14

Molecular Modeling of the Transmembrane Domain of the SARS Cov-2 S-Protein and its Interaction with the Membrane

Valery Novoseletsky, Marine Bozdaganyan, Daniil Litvinov, Olga Sokolova

M. V. Lomonosov Moscow State University, Moscow, Russia

Background: The spike glycoprotein of SARS-coronavirus mediates the early events leading to infection of cells, including fusion of the viral and cellular membranes. The spike is a type I membrane glycoprotein that possesses a conserved transmembrane anchor and an unusual cysteine-rich domain that bridges the putative junction of the anchor and the cytoplasmic tail. In this study, we examined the role of these carboxyl-terminal domains in S-protein interaction with membrane.

Methods: Structural model of the trimeric TM domain and adjacent fragments of ecto- and endo domains (residues 1157-1256) of the S-protein was built by homology basing on the solution structure of the SARS-coronavirus S-protein HR2 domain (pdb-code 2fxp), the structure of the transmembrane domain of HIV-1 gp41 in bicelle (5jyn), and assumption of generally coiled-coil fold of the considered domain. C-terminus of the domain was left unstructured but fully palmitoylated. Molecular dynamics simulation in heterogeneous lipid bilayer was prepared with CHARMM-GUI and performed with Gromacs during 100 ns.

Results: 1. Ectodomain fragment (residues 1157-1212) demonstrates a tilt by the angle of 40-60 degrees from the axis of the TM domain (residues 1213-1237). This tilt is facilitated by glycine residues in position 1204. 2. Cholesterol molecules

of the bottom layer tend to localize around protein due to interaction with palmitoyl tails while lipids in the upper layer do not show such tendency.

Conclusion: Performed molecular simulations show that both palmitoylation and a large cluster of aromatic residues provide high stability of the S-protein TM domain.

Key Words: SARS Cov-2, S-protein, palmitoylation, molecular modeling

This work was supported by the Russian Foundation for Basic Research (Grant No. 20-04-60258)

***Corresponding author:** Valery Novoseletsky. E-mail: valery.novoseletsky@yandex.ru

P-15

http://dx.doi.org/10.21103/IJBM.11.Suppl_1.P15

Cryo-Electron Microscopy Study of Dehydrogenase Complexes Interaction with Oxidative Phosphorylation System Supercomplex

Konstantin Plokhikh¹, Roman Kamyshinsky¹, Yury Chesnokov¹, Semen Nesterov^{1,2}, Raif Vasilov^{1,3}, Lev Yaguzhinsky^{2,3,4}

¹National Research Center "Kurchatov Institute," Moscow, Russia

²Moscow Institute of Physics and Technology, Dolgoprudny, Russia

³Belozersky Research Institute for Physico-Chemical Biology, Moscow, Russia

⁴Institute of Cytochemistry and Molecular Pharmacology, Moscow, Russia

Background: Electron transport chain (ETC) complexes, pyruvate dehydrogenase complex (PDC), and α -ketoglutarate dehydrogenase complex (KGDC) are important elements in mitochondrial metabolism. The localization of the aforementioned protein complexes differs since oxidative phosphorylation complexes are membrane proteins, while dehydrogenase complexes (DCs) are contained in the mitochondrial matrix. Our previous cryo-electron tomography (cryo-ET) studies showed the existence of a full oxidative phosphorylation system supercomplex consisting of ETC complexes and ATP synthases (Nesterov et al., 2021). Literature data also shows the binding of fatty acid oxidation enzymes to ETC complex I (Wang et al., 2010). Although it has long been shown that PDCs can bind to complex I (Sumegi et al., 1984) in vitro, this has not been visualized directly in mitochondria and the binding mechanisms are still unknown.

Methods: The mitochondria were isolated from Wistar rat heart ventricles according to a standard procedure (Nesterov et al., 2021). The dense mitochondrial suspension was diluted to ~0.3mg/ml in a respiration medium. Phosphorylation was started 10 minutes prior to vitrification. Experimental data was obtained by cryo-ET using Titan Krios and processed with IMOD and RELION.

Results: The tomograms show that the significant part of DCs is localized near the inner membrane of partially destroyed mitochondria in an array-like fashion. Sole PDCs and KGDCs can be identified on the images and their position appears to be close to ETC complex I. Subtomogram averaging of close to the membrane DCs showed that there is no specific density between them, suggesting that they are not linked with identical proteins or that this link may be soft. Significant damage to the mitochondrial membrane leads to the formation of membrane-unbound DCs fraction. It suggests that coupling of DCs with

ETC complexes can be controlled in vivo by the topology of the inner mitochondrial membrane and the volume of the mitochondrial matrix.

Conclusion: The obtained results show a possibility of unprecedentedly large multienzyme complex formation, including almost all main mitochondrial metabolic systems. Although cryo-ET of partially destroyed mitochondria showed close localization of PDC and KGDC to complex I, further studies are required in intact mitochondria. The mechanism of their binding also remains an open question.

Key Words: cryo-ET, pyruvate dehydrogenase complex, α -ketoglutarate dehydrogenase complex, oxidative phosphorylation

This work was supported by the Russian Foundation for Basic Research (Grant No. 19-04-00835) and NRC "Kurchatov Institute" (thematic plan "Study of the processes of generation, transmission and distribution of energy in living organisms")

***Corresponding author:** Konstantin Plokhikh. E-mail: konstantin.plokhikh@phystech.edu

P-16

http://dx.doi.org/10.21103/IJBM.11.Suppl_1.P16

Cryo-Electron Microscopy Study of Vesicles from Various Species

Evgeny V. Yastremsky¹, Luiza A. Garaeva^{1,2}, Elena D. Putevich², Dmitry A. Sazonov³, Alexander L. Vasiliev^{1,3}, Roman A. Kamyshevsky^{1,3}, Tatiana A. Shtam^{1,2}

¹National Research Center "Kurchatov Institute," Moscow, Russia

²Petersburg Nuclear Physics Institute named by B.P. Konstantinov of NRC "Kurchatov Institute," Gatchina, Russia

³Shubnikov Institute of Crystallography of FSRC "Crystallography and Photonics" RAS, Moscow, Russia

⁴Saint Petersburg State University, St. Petersburg, Russia

Background: Plant-derived extracellular vesicles (PEVs) are studied as a natural carrier of functional biomolecules and as a potential system of targeted delivery of therapeutic agents. One of the urgent tasks in this direction is the selection of the carrier with optimal physicochemical parameters and morphology from a variety of plant sources. To date, vesicles from only a few plants were visualized using cryo-electron microscopy (cryo-EM). Here we investigated the morphology and physical parameters of extracellular vesicles from plant sources not previously studied utilizing this method.

Methods: PEVs derived by ultracentrifugation from juice and cultural medium of 11 plants and mushrooms were studied using methods of cryo-EM. Samples were plunge frozen in liquid ethane with Vitrobot Mark IV and examined under cryogenic transmission electron microscope Titan Krios 60-300 (ThermoFisher Scientific, USA) in low dose mode using EPU software

Results: Most of the observed particles in each sample were classified as extracellular vesicles due to the presence of the lipid bilayer. Morphology and size characteristics of PEVs were determined and compared with each other. A variety of morphological configurations of PEVs were found: with single and multiple membranes, with different conformations and integrity state. Most of the isolated PEVs were single, round-shaped, and in a size range from 30 to 150 nm.

Conclusion: Cryo-EM allowed us to obtain high-quality images of PEVs isolated from 11 plants and mushrooms

(blueberry, chanterelle, cowberry, fly agaric, garlic, redcurrant, *chlamydomonas*, cucumber, shadberry, viburnum, gooseberry) which have been characterized by their size and morphology. From the data obtained, the most promising sources of vesicles were proposed. The approbation of the selected vesicles as effective delivery systems requires further research.

Key Words: cryo-EM; extracellular vesicles; plant-derived extracellular vesicles

This work was supported by the Russian Science Foundation (Grant No. 19-74-20146)

***Corresponding author:** Evgeny V. Yastremsky. E-mail: e.yastremsky@gmail.com

P-17

http://dx.doi.org/10.21103/IJBM.11.Suppl_1.P17

Photophysical Properties of Freely Diffusing and Immobilized Fluorescent Conjugate Based on Calcium-Binding Protein Recoverin and Alexa647 Dye

Iliia Zykov¹, Ivan Maslov¹, Evgeni Zernii^{2,3}, Sergei Permyakov⁴, Thomas Gensch⁵, Valentin Borshchevskiy¹

¹Moscow Institute of Physics and Technology, Dolgoprudny, Russia

²Lomonosov Moscow State University, Moscow, Russia

³Sechenov First Moscow State Medical University, Moscow, Russia

⁴Federal Research Center "Pushchino Scientific Center for Biological Research of the Russian Academy of Sciences," Pushchino, Russia

⁵Forschungszentrum Jülich, Jülich, Germany

Background: Recoverin is a calcium sensor membrane-associated protein that inhibits rhodopsin kinase thereby participating in the regulation of visual transduction. Here we examined calcium-induced conformational changes in recoverin conjugated with fluorescent dye Alexa647.

Methods: Photophysical properties of immobilized and freely diffusing recoverin were investigated using fluorescence lifetime imaging microscopy and fluorescence emission spectroscopy. In solution, the formation and dissociation of the Ca²⁺-recoverin complex manifested as changes in Alexa647 spectra and the lifetime. In contrast, immobilization of recoverin on the microscopy glass via biotin-NeutrAvidin-biotinylated polyethylene glycol (PEG) tether inhibited changes in fluorescent signal. That can be provided by PEG as it prevented the calcium-induced changes in spectrum and lifetime of recoverin-bound Alexa647 in solution. The use of another immobilization facilitator, bovine serum albumin (BSA), did not affect calcium-induced changes in fluorescence of the conjugate in solution but produced the matrix, which was ineffective in recoverin immobilization.

Results: Microscale thermophoresis demonstrated that biotinylated recoverin interacted with NeutrAvidin in solution indicating that immobilization affinity depended mainly on the geometry of the glass coating surface.

Conclusion: Our results highlight the challenge of specific protein immobilization that does not affect protein functionality. By the example of recoverin, we showed that the employment of two common immobilization facilitators, PEG and BSA, yielded surfaces with different space geometry, which differently affect NeutrAvidin-based immobilization affinity as well as Ca²⁺-dependent conformational changes of the biotinylated protein.

Key Words: Recoverin, microscale thermophoresis, protein immobilization

This work is supported by the Ministry of Science and Higher Education of the Russian Federation (agreement #075-00337-20-03, project FSMG-2020-0003)

***Corresponding author:** Iliia Zykov. E-mail: zykov.io@phystech.edu

STRUCTURE AND FUNCTIONS OF THE TRANSCRIPTION AND TRANSLATION APPARATUS OF THE CELL

P-18

http://dx.doi.org/10.21103/IJBM.11.Suppl_1.P18

Phosphorylation of RNA Polymerase II C-Terminal Domain Affects Transcript Elongation Through Chromatin

Sohail Akhtar¹, Elena Y. Kotova², Nadezhda S. Gerasimova³, Vasily M. Studitsky^{2,3}

¹*Molecular and Structural Biology Division, Council of Scientific and Industrial Research (CSIR)-Central Drug Research Institute, Lucknow, India*

²*Fox Chase Cancer Center, Philadelphia, PA, USA*

³*Biology Faculty, Lomonosov Moscow State University, Moscow, Russia*

Background: Transcription is the central point of gene regulation where the efficient maintenance of chromatin structure during the passage of RNA polymerase (Pol II) is critical for cell survival and functioning. The phosphorylation of carboxy-terminal domain (CTD) of the large subunit (Rpb1) of Pol II plays a key role in transcription through chromatin providing the binding and dissociation of factors essential for the mRNA biogenesis. Although the regulatory effect of chromatin structure on multiple stages of transcription has been well established, the role of CTD phosphorylation itself has not been systematically addressed.

Methods: The effect of differentially phosphorylated Pol II-CTD on transcript elongation through chromatin was studied using in vitro transcription system based on mononucleosomes precisely positioned on DNA. The unphosphorylated and hyperphosphorylated Pol II-CTD were obtained using yeast genetics as well as in vitro kinase or phosphatases. Transcription rate and positions of pausing were measured using authentic elongation complexes comprising Pol II having different CTD phosphorylation states. The quantitative analysis of the transcripts was conducted using denaturing PAGE.

Results: We observed a significant difference in the transcription through chromatin depending on CTD phosphorylation level. Thus, experiments on transcription of nucleosomes with Pol II isoforms have shown that the hyperphosphorylated form more efficiently transcribes the nucleosome and leads to a faster accumulation of the full-length RNA product than the non-phosphorylated isoform of Pol II. The non-phosphorylated isoform of the enzyme is characterized by a stronger pause in the early nucleosomal region and a slower accumulation of the full-length RNA product.

Conclusion: Hyperphosphorylated form more efficiently transcribes the nucleosome and leads to a faster accumulation of the full-length RNA product as compared with the non-phosphorylated isoform of Pol II. A preliminary model of the effect of Pol II hyperphosphorylation on nucleosomal DNA transcription is proposed.

Key Words: RNA polymerase, transcription, nucleosome, C-terminal domain

This work was supported by the Russian Scientific Foundation (project No. 19-44-02013 to V.M.S.) and the Department of Science and Technology, India (Bilateral Grant Project Code No. GAPO330 to S.A.)

***Corresponding author:** Sohail Akhtar. E-mail: sohail@cdri.res.in

P-19

http://dx.doi.org/10.21103/IJBM.11.Suppl_1.P19

15-Microsecond Molecular Dynamics Simulations of Nucleosome Show Structural Heterogeneity and Plasticity

Grigoriy A. Armeev¹, Anastasiia S. Kniazeva¹, Galina A. Komarova³, Mikhail P. Kirpichnikov^{1,4}, Alexey K. Shaytan^{1,2,5}

¹*Department of Biology, Lomonosov Moscow State University, Moscow, Russia*

²*Sirius University of Science and Technology, Sochi, Russia*

³*Department of Physics, Lomonosov Moscow State University, Moscow, Russia*

⁴*Shemyakin-Ovchinnikov Institute of Bioorganic Chemistry, Russian Academy of Sciences, Moscow, Russia*

⁵*Bioinformatics Lab, Faculty of Computer Science, HSE University, Moscow, Russia*

Background: Nucleosomes are basic units of chromatin organization, resembling spools with ~150 base pairs of DNA wrapped around the octamer of histone proteins. They play a crucial role in chromatin compactization and gene expression. Currently, there are more than 340 structures of nucleosomes and their complexes with proteins in the protein data bank, 159 of them are made with cryoEM, 60 of those in 2020 and later. It is clear that cryoEM will soon yield even more structures of nucleosomes with different histone variants, mutations, DNA sequences, and interacting proteins. Despite the variety, the majority of the aforementioned structures look very similar. This is due to the fact that most of the models are built on the basis of very similar crystal structures. However, the dynamics of nucleosomes are crucial for understanding the mechanisms that govern the chromatin functions. Computational methods can supplement experimental approaches and recreate the dynamic conformational landscape of nucleosomes from initial static structures. We present an all-atom molecular dynamics simulation of nucleosome core particles at a record timescale of 15 microseconds.

Methods: All-atom MD simulations were performed using GROMACS 2018 with AMBER ff14SB force field with parmbsc1 DNA and CUFIX ion parameters. Crystal structures with PDB IDs 1KX5 and 3LZ0 were used. Analysis was performed with custom-developed python scripts based on MDAnalysis and 3DNA. Models of chromatin fibers were built by connecting random snapshots from MD trajectories with straight linker segments of B-DNA of different lengths.

Results: We observed the inner dynamics of histone octamer, which covers the conformational space of the most deformed structures reported by cryoEM. We showed that histone dynamics play important role in DNA mobility, allowing for twist-defects propagation.

Conclusion: We observed unprecedented unwrapping of nucleosomal DNA with truncated histone tails. Through multi-scale modeling, we showed that such unwrapping alone is crucial for nucleosomal fibers geometry and elastic properties.

Key Words: nucleosome, chromatin, molecular dynamics

This work was supported by the Russian Science Foundation (Grant No. 18-74-10006)(MD simulations and analysis), RFBR grants (Grant No. 20-34-70039) (supranucleosome structure modeling), (Grant No. 19-34-51053) (development of protein-DNA analysis algorithms) and by the Interdisciplinary Scientific and Educational School of Moscow University "Molecular Technologies of the Living Systems and Synthetic Biology." A.K.S is supported by the HSE University Basic Research Program. The research was carried out using the equipment of the shared research facilities of HPC computing resources at Lomonosov Moscow State University.

*Corresponding author: Grigoriy Armeev. E-mail: armeev@intbio.org

P-20

http://dx.doi.org/10.21103/IJBM.11.Suppl_1.P20

Sub 3 Resolution Cryo-EM Structure of Eukaryotic Small (40S) Ribosomal Subunit

Timur N. Baymukhametov¹, Olesya V. Kravchenko², Zhanna A. Afonina², Konstantin S. Vassilenko²

¹National Research Center, "Kurchatov Institute," Moscow, Russia

²Institute of Protein Research, Russian Academy of Sciences, Pushchino, Russia

Background: The ribosome is a molecular machine that translates mRNAs into proteins. In eukaryotes, ribosome consists of small (40S) and large (60S) subunits. Translation in eukaryotes is a complicated molecular process that involves the formation of various molecular complexes consisting of ribosomal subunits and protein factors. Cryo-EM approaches such as single particle analysis are widely used for structural analysis of components and intermediates of the translation machinery. However, the process of translation in plants is still poorly characterized at a structural level. Here, we present the structure of *Triticum aestivum* small ribosomal subunit obtained at sub 3 resolution that can be used for further structural studies of the translation process in plants.

Methods: The structures of the 40S subunits purified from wheat germ extract were obtained using high-resolution single particle cryo-EM. For cryo-EM sample preparation were used Quantifoil R 1.2/1.3 grids coated with an additional 2 nm amorphous carbon film were glow-discharged for 30 seconds at 15 mA using PELCO easiGlow (Ted Pella). 3 μ L of the sample were applied onto the grids, blotted for 3 sec at 10°C and 100% humidity, and plunge-frozen in liquid ethane using Vitrobot Mark IV (Thermo Fisher).

Cryo-EM data were collected using a Cs-corrected Titan Krios (Thermo Fisher) transmission electron microscope, equipped with a Falcon II direct electron detector. Data were acquired with defocus range of -0.6 to -2.0 at a nominal magnification of 75,000x, giving a calibrated pixel size of 0.86 Å/pixel. The micrographs were recorded as movie stacks. The exposure time for each stack was 1.6 s, corresponding to a total electron dose of ~84 e-/Å² fractionated into 32 frames (~2.6 e-/Å² per single frame). A total of 5521 movie stacks was collected. Raw cryo-EM data preprocessing was performed with Warp software (Tegunov et al., 2019). All further data processing steps were performed using the cryoSPARC v3.2.0 software (Punjani et al., 2017).

Results: For final cryo-EM map refinement, 140,000 particles were used resulting in 2.7 Å resolution estimated using an FSC=0.143 gold-standard threshold. The obtained structural data clearly demonstrate the peculiarities of the

spatial organization of the 40S ribosomal subunit, like the motility of the head relative to the body revealed by 3D variability analysis.

Conclusion: The resulting structure was solved at a significantly higher resolution compared to the previously published structure of a plant ribosome (Armache et al., 2010) and will be used as a reference for further studies of translation initiation in plants.

Key Words: cryo-EM, 40S ribosomal subunit.

This work was supported by the Russian Science Foundation (Grant No. 19-74-20186)

*Corresponding author: Timur N. Baymukhametov. E-mail: baymukhametov.timur@gmail.com

P-21

http://dx.doi.org/10.21103/IJBM.11.Suppl_1.P21

The Investigation of *S. aureus* Ribosome-Binding Factor A Localization on the 30S Ribosomal Subunit by Cryo-Electron Microscopy

Aydar G. Bikmullin¹, Artem Stetsenko², Alexander Golubev^{1,3}, Liliia Nurullina³, Iskander Khusainov⁴, Evelina Klochkova¹, Natalia Garaeva¹, Konstantin Usachev¹

¹Kazan Federal University, Kazan, Russia

²University of Groningen, Groningen, the Netherlands

³Institut de Génétique et de Biologie Moléculaire et Cellulaire, Université de Strasbourg, Illkirch, France

⁴Department of Molecular Sociology, Max Planck Institute of Biophysics, Frankfurt am Main, Germany

Background: Ribosome biogenesis is a complex process of ribosomal RNA and protein binding. Bacterial ribosome maturation and components involved in it are especially interesting, because they are widespread targets for antibiotics. A number of special protein factors facilitating the maturation of the 30S small ribosomal subunit are known. One of them is a ribosome-binding factor A (RbfA). This is a small (~14 kDa) protein with KH-domain organization distinguishing RNA binding proteins. Recent cryo-EM reconstruction of E.coli 30S-RbfA complex indicates that RbfA binds to 30S subunit on the central decoding region and promotes the switch from the immature state of h28 (neck) to mature state. RbfA interacts with 3'-end of 16S rRNA on mRNA exit channel and stabilizes the conformation of the region between h28, h44/h45 linker and 3'-end.

Methods: Pure *S.aureus* RbfA was obtained by homologous expression in E.coli BL21 strain followed by Ni-NTA and gel filtration. The 30S subunits were obtained by dissociation of the *S.aureus* 70S ribosomes in a sucrose gradient (0-30%). We performed 30S subunit and RbfA complex reconstitution, sample and grid preparation. Data was collected on Talos Arctica, Falcon 2 detector (FEI Company/Thermo Fisher).

Results: The 30S-RbfA complex density map with average resolution ~ 3.5 Å (FSC=0.143) was obtained. In comparison with the free subunit map (EMD 23052) we observed an extra density on the neck region near the decoding center region.

Conclusion: Obtained data is correlated with recent structural results of the homologous E.coli RbfA. We consider that *S.aureus* RbfA binds to the 30S subunit at the same region. The next step of our structural research is building the model of *S.aureus* 30S-RbfA complex.

Key words: Ribosome, 30S subunit biogenesis, RbfA, protein translation

This work was supported by the Russian Foundation for Basic Research (Grant No. 20-54-15001)

*Corresponding author: Aydar G. Bikmullin. E-mail: aydar.bikmullin@gmail.com

P-22

http://dx.doi.org/10.21103/IJBM.11.Suppl_1.P22

Enhanced Crosslinking and Immunoprecipitation (Eclip) Data Reveal Interactions of RNA Binding Proteins with the Human Ribosome

Andrey Buyan^{1,2}, Ivan V. Kulakovskiy^{1,3,4}, Sergey E. Dmitriev^{1,2,3}

¹Belozersky Institute of Physico-Chemical Biology, Lomonosov Moscow State University, Moscow, Russia

²Faculty of Bioengineering and Bioinformatics, Lomonosov Moscow State University, Moscow, Russia

³Engelhardt Institute of Molecular Biology, Russian Academy of Sciences, Moscow, Russia

⁴Institute of Protein Research, Russian Academy of Sciences, Pushchino, Russia

Background: The ribosome is a protein-synthesizing molecular machine composed of four ribosomal RNAs (rRNAs) and dozens of ribosomal proteins. In mammals, the ribosome has a complicated structure with an additional outer layer of rRNA, including large tentacle-like extensions. A number of RNA binding proteins (RBPs) interact with this layer to assist ribosome biogenesis, nuclear export and decay, or to modulate translation. Plenty of methods have been developed in the last decade in order to study such protein-RNA interactions, including RNA pulldown and crosslinking-immunoprecipitation (CLIP) assays.

Methods: In the current study, using publicly available data of the enhanced CLIP (eCLIP) experiments for 223 proteins studied in the ENCODE project, we found a number of RBPs that bind rRNAs in human cells. To locate their binding sites in rRNAs, we used a newly developed computational protocol for mapping and evaluation of the eCLIP data with the respect to the repetitive sequences.

Results: For two proteins with known ribosomal localization, uS3/RPS3 and uS17/RPS11, the identified sites were in good agreement with structural data, thus validating our approach. Then, we identified rRNA contacts of overall 22 RBPs involved in rRNA processing and ribosome maturation (DDX21, DDX51, DDX52, NIP7, SBDS, UTP18, UTP3, WDR3, and WDR43), translational control during stress (SERBP1, G3BP1, SND1), IRES activity (PCBP1/hnRNPE1), and other translation-related functions. In many cases, the identified proteins interact with the rRNA expansion segments (ES) of the human ribosome pointing to their important role in protein synthesis.

Conclusion: Our study identifies a number of RBPs as interacting partners of the human ribosome and sheds light on the role of rRNA expansion segments in translation.

Key Words: RNA-binding proteins, rRNA expansion segments, 40S and 60S ribosomal subunits, eCLIP.

This work was supported by the Russian Science Foundation (Grant No. 18-14-00291)

*Corresponding author: Andrey Buyan. E-mail: andreybuyanchik@gmail.com

P-23

http://dx.doi.org/10.21103/IJBM.11.Suppl_1.P23

Histone N-terminal Tails Reduce Early Nucleosomal Pausing during Transcription

Nadezhda S. Gerasimova¹, Fu-Kai Hsieh², Vasily M. Studitsky^{1,2}

¹Biology Faculty, Lomonosov Moscow State University, Moscow, Russia

²Fox Chase Cancer Center, Philadelphia, Pennsylvania, USA

Background: Nucleosomes are the barriers to transcript elongation by RNA polymerase 2 (Pol 2) *in vitro* and *in vivo*. Formation and overcoming the barrier are important for transcription regulation. N-terminal tails of core histones do not affect the inner structure of nucleosomal core. However, strongly positively charged tails can interact with the DNA, thereby impeding polymerase progression through the template. Removal of histone tails was shown to facilitate transcription through a nucleosome by both yeast and human Pol 2, and the effect was most noticeable at lower ionic strength (40 mM KCl). *In vivo* experiments established a new mechanism of overcoming of +1 nucleosomal barrier by removal of histone tails by specific regulative proteinase. As +1 nucleosomal barrier is formed mostly by the promoter-proximal part of the nucleosomal DNA, here we address the effects of histone tails on elongation through this part of the nucleosome.

Methods: We have studied the effect of histone tails on transcription by yeast Pol 2 and model enzyme *E. coli* RNA polymerase utilizing very similar mechanisms of elongation through chromatin. 603 nucleosomes were transcribed *in vitro* using purified proteins and components. To focus on the proximal part of the nucleosome, transcript elongation was conducted for a limited time and at low ionic strength.

Results For the phosphorylated form of yeast Pol 2 and *E. coli* RNAP, histone tail removal significantly reduces the strong nucleosome-specific pausing that the yeast polymerase encounters ~15 bp within the 603 nucleosome and further downstream, leading to both increased traversal of the pause and the accumulation of complexes paused at more distal locations. However, tail removal did not lead to a significant increase in full traversal of either nucleosomal template. The effect of histone tails removal was cognate for both enzymes but differs in detailed effect on the barrier.

Conclusions: Histone tails provide a significant part of the nucleosomal barrier to transcript elongation by Pol 2-type mechanism. The effect is very pronounced in the promoter-proximal part of the nucleosomal DNA, suggesting that histone tails could play a role during the regulation of the +1 nucleosomal barrier. The role of Pol 2 CTD phosphorylation and formation of the intranucleosomal loops in the regulation of +1 nucleosomal barrier will also be addressed.

Key Words: RNA polymerase, transcription, nucleosome, histone tails

This work was supported by the Russian Scientific Foundation (Grant No. 19-44-02013)

*Corresponding author: Nadezhda S. Gerasimova. E-mail: gerasimova@mail.bio.msu.ru

P-24

http://dx.doi.org/10.21103/IJBM.11.Suppl_1.P24

Microscopic Analyses of Liquid-Liquid Phase Separation Induced by Linker Histone H1.0

Olga Geraskina^{1,2}, Natalya Maluchenko¹, Vasily Studitsky^{1,3}, Nadezhda Gerasimova¹, Daria Koshkina^{1,2}, Alexey Feofanov^{1,2,4}

¹Faculty of Biology, Lomonosov Moscow State University, Moscow, Russia

²Institute of Gene Biology, Russian Academy of Sciences, Moscow, Russia

³Fox Chase Cancer Center, Philadelphia, USA

⁴Shemyakin-Ovchinnikov Institute of Bioorganic Chemistry, Russian Academy of Sciences, Moscow, Russia

Background: Liquid-liquid phase separation (LLPS) that leads to the formation of temporary functional domains in cells plays an important role in the processes of chromatin condensation and gene regulation. Earlier, it was demonstrated that histone H1.4 can form LLPS droplets with DNA. In the present work, LLPS was studied for histone H1.0, which is mainly expressed in differentiated and non-dividing cells. H1.0 is involved in cancer development: its amount decreases with the progression of tumor cells to malignancy.

Methods: LSM710 confocal microscope (Zeiss) equipped with the 40x/1.2W objective was used to image mixtures of H1.0 with Cy3/Cy5 labeled DNA or nucleosomes in fluorescent and transmitted-light channels at the excitation of 514 nm. The formation of condensates as a result of LLPS was confirmed by salt-jump and FRAP/FLIP experiments.

Results: Condensates were not observed when the ratio of negative to positive charges (N/P) in the samples was >1. At N/P~0.7, optically homogeneous droplet-like condensates were found. The appearance of condensates, their size and shape depended on concentrations of H1.0 and DNA. LLPS condensates but not aggregates disappeared by salt-jump to 650 mM NaCl. FRAP/FLIP experiments revealed a moderate rate of fluorescence recovery ($\tau_{1/2}$ ~22s) indicating moderate DNA mobility of the H1.0-mediated condensates. The appearance of condensates was also observed in the mixtures of H1.0, DNA and Cy3/Cy5-labeled nucleosomes. Nucleosomes were involved in the condensate formation and found to be 2-fold more mobile ($\tau_{1/2}$ ~10 s) than DNA.

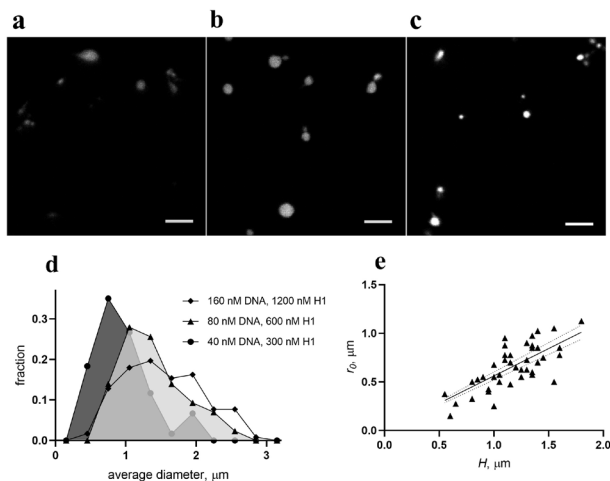


Figure. Liquid-liquid phase separation of Cy3/Cy5-labelled DNA and nucleosomes induced by H1.0. Fluorescent images of condensates formed upon mixing: (a) 300 μ M H1.0 and 40 nM DNA, (b) 1.2 μ M H1 and 160 nM DNA, (c) 10 nM nucleosomes, 70 nM DNA, 600 nM H1.0. Bar size is 5 μ m. (d) Distribution of condensates in specimens by size. (e) Graph of the relationship between the height (H) and the radius of a base (r_0) of an immobilized condensate for a sample of condensates in specimen (b). Straight line - linear regression of data.

Conclusion: LLPS-related properties of H1.0 were studied for DNA and nucleosomes in vitro. Comparison with H1.4

shows that H1.0 forms liquid condensates of approximately the same size. Our result also may indicate that chromatin retains pronounced dynamic properties in H1.0-induced droplets despite the fact that H1.0 induces the formation of more compact chromatin.

Key Words: LLPS, DNA, Nucleosome, H1.0.

This work was supported by the Russian Science Foundation (Grant No. 21-64-00001).

*Corresponding author: Olga Geraskina. E-mail: olgsamsonova@yandex.ru

P-25

http://dx.doi.org/10.21103/IJBM.11.Suppl_1.P25

High-Resolution Cryo-Electron Microscopy Structure of the Staphylococcus Aureus Ribosome Brings to Light New Possible Drug Targets

Alexander Golubev¹, Bulat Fatkhullin², Iskander Khusainov³, Shamil Validov⁴, Marat Yusupov¹, Konstantin Usachev⁴

¹Département de Biologie et de Génomique Structurales, Institut de Génétique et de Biologie Moléculaire et Cellulaire, Université de Strasbourg, Illkirch, France

²Institute of Protein Research, Russian Academy of Sciences, Puschino, Russia

³Department of Molecular Sociology, Max Planck Institute of Biophysics, Frankfurt am Main, Germany

⁴Laboratory of Structural Biology, Institute of Fundamental Medicine and Biology, Kazan Federal University, Kazan, Russia

Background: Antibiotic resistance is a growing worldwide problem. One of the major resistant bacterial pathogens is *Staphylococcus aureus*, which became a burden of healthcare systems around the world. To overcome the issue, more drug discovery studies are needed. One of the main antibiotic targets is a ribosome – the central hub of protein synthesis. Structural data of the ribosome and its features are a crucial milestone for the effective development of new drugs, especially using structure-based drug design approaches. Apart from many small structural features, ribosome possesses rRNA modifications that play a role in the fine-tuning of protein synthesis. Detailed species-specific structural data of the *S. aureus* ribosome is also a useful model for understanding the resistance mechanisms. This information could help with the design of new antibiotics and the upgrading of old ones. The data on *S. aureus* ribosomal RNA modifications and corresponding modification enzymes are very limited. Our aim was to improve the current models of the *S. aureus* ribosome by determining its structure with functional ligands at a much higher resolution - thereby creating a foundation for structure-based drug design experiments and research of new drug targets.

Methods: The *S. aureus* ribosome complex consists of three components: ribosome, fMet-tRNA^{fMet}, mRNA and 70S ribosome. The complex from purified components was formed in vitro and applied to cryo-EM grids. Data was collected at Titan Krios with Gatan K2 detector (IGBMC, France). The data was processed and modeled in Relion 2.1, Chimera, Coot, and Phenix.

Results: We determined the cryo-EM reconstruction at 3.2 Å resolution of the *S. aureus* ribosome with P-site tRNA, messenger RNA. Based on the experimental map and existing bioinformatic data, we at the first time identified and assigned 10 modifications of *S. aureus* rRNA. We analyzed the positions of rRNA modifications and their possible functions.

Conclusion: In this study, we describe our structure of *S. aureus* ribosome with functional ligands. The present model is the highest resolution and most precise that is available at the moment. We propose a set of methyltransferases as targets for future drug discovery studies. The proposed methyltransferases and corresponding modifications may play an important role in protein synthesis and its regulation.

Key Words: ribosome, cryo-EM, rRNA modifications, *S. aureus*

***Corresponding author:** Alexander Golubev. E-mail: golubeva@igbmc.fr

P-26

http://dx.doi.org/10.21103/IJBM.11.Suppl_1.P26

***Staphylococcus Aureus* 30S Ribosomal Subunit in a Complex with the Era GTPase: Sample Preparation for Cryo-EM**

Evelina Klochkova¹, Aydar Bikmullin¹, Shamil Validov¹, Natalia Garaeva¹, Marat Yusupov², Konstantin Usachev¹

¹*Institute of Fundamental Medicine and Biology, Kazan Federal University, Kazan, Russia*

²*Institut de Génétique et de Biologie Moléculaire et Cellulaire, Université de Strasbourg, Illkirch, France*

Background: An essential in bacteria GTPase Era is a multifunctional protein that is involved in cell cycle regulation and appears to play a significant role in ribosome biogenesis. It is required for the maturation of the 30S ribosomal subunit.

Era consists of two domains: the GTPase N-terminal domain, conserved in the GTPase family, and a C-terminal RNA-binding KH domain. Era specifically binds to the 16S rRNA and stimulates processing of the small ribosomal subunit to its mature form.

Precise determination of nucleotide and amino acid sequences in the active site of binding will help in finding specific ways to prevent this interaction. In this way, it will be possible to disrupt the biogenesis of the ribosome and, thereby, stop or slow down protein synthesis in the bacterial cell. It is very important in the fight against pathogenic bacteria, such as *Staphylococcus aureus* (*S. aureus*).

Methods: The His-tagged Era (His-Era) protein from *S. aureus* was expressed in *E. coli* BL21 strain and purified by Ni-NTA and SEC. The 30S ribosomal subunits were collected after dissociation of the *S. aureus* 70S ribosomes in sucrose gradient (0 – 30%). Complex 30S-Era was obtained by mixing in vitro 30S subunits and His-Era, incubated for 15 min at 37°C and followed by Ni-NTA purification to remove unbound 30S subunits. The presence of a stable 30S-Era complex has been confirmed by SDS-PAGE and agarose gel electrophoresis. The final sample quality was analyzed by negative staining EM.

Results: For the first time in vitro 30S-Era complex from *S. aureus* was assembled and a sample was prepared for further structural studies by cryo-electron microscopy.

Key Words: GTPase, Era, ribosome, 30S subunit, *Staphylococcus aureus*

This work was supported by the Russian Science Foundation (Grant No. 21-74-20034).

***Corresponding author:** Evelina Klochkova. E-mail: evelina.klochkova@gmail.com

P-27

http://dx.doi.org/10.21103/IJBM.11.Suppl_1.P27

The 30S Ribosomal Subunit Assembly Factor RbfA Plays a Key Role in the Formation of the Central Pseudoknot and in the Correct Docking of Helix 44 of the Decoding Center

Elena M. Maksimova¹, Alexey P. Korepanov¹, Olesya V. Kravchenko¹, Timur N. Baymukhametov², Alexander G. Myasnikov^{3,4}, Konstantin S. Vassilenko¹, Zhanna A. Afonina¹, Elena A. Stolboushkina¹

¹*Institute of Protein Research, Russian Academy of Sciences, Pushchino, Russia*

²*National Research Center, "Kurchatov Institute," Moscow, Russia*

³*Petersburg Nuclear Physics Institute named by B.P. Konstantinov of NRC "Kurchatov Institute," Gatchina, Russia*

⁴*Department of Structural Biology, St. Jude Children's Research Hospital, Memphis, Tennessee, USA*

Background: Ribosome biogenesis is a complicated multi-stage process. In the cell, 30S ribosomal subunit assembly is fast and efficient, proceeding with the help of numerous assembly protein factors. The exact role of most assembly factors and mechanistic details of their operation remain unclear. The combination of genetic modification with cryo-EM analysis is widely used to identify the role of protein factors in assisting specific steps of the ribosome assembly process. The strain with knockout of a single assembly factor gene accumulates immature ribosomal particles which structural characterization reveals the information about the reactions catalyzed by the corresponding factor.

Methods: We isolated the immature 30S subunits (pre-30S subunits) from the *Escherichia coli* strain lacking the *rbfA* gene (*ArbFA*) and characterized them by cryo-electron microscopy (cryo-EM).

Results: Deletion of the assembly factor RbfA caused a substantial distortion of the structure of an important central pseudoknot which connects three major domains of 30S subunit and is necessary for ribosome stability. It was shown that the relative order of the assembly of the 3' head domain and the docking of the functionally important helix 44 depends on the presence of RbfA. The formation of the central pseudoknot may promote stabilization of the head domain, likely through the RbfA-dependent maturation of the neck helix 28. The cryo-EM maps for pre-30S subunits were divided into the classes corresponding to consecutive assembly intermediates: from the particles with completely unresolved head domain and unfolded central pseudoknot to almost mature 30S subunits with well-resolved body, platform, and head domains and with partially distorted helix 44. Cryo-EM analysis of *ArbFA* 30S particles revealing the accumulation of two predominant classes of early and late intermediates (obtained at 2.7 Å resolutions) allowed us to suggest that RbfA participate in two stages of the 30S subunit assembly and is deeper involved in the maturation process than previously thought.

Conclusion: In summary, RbfA acts at two distinctive 30S assembly stages: early formation of the central pseudoknot including the folding of the head, and positioning of helix 44 in the decoding center at a later stage. An update to the model of factor-dependent 30S maturation was proposed, suggesting that RbfA is involved in most of the subunit assembly process.

Key Words: ribosome assembly, cryo-EM, 30S subunit maturation, RbfA

This work was supported by the Russian Science Foundation (Grant No. 19-74-20186 to Zh.A.A.).

***Corresponding author:** Elena M. Maksimova. E-mail: elena.maks.89@gmail.com

P-28

http://dx.doi.org/10.21103/IJBM.11.Suppl_1.P28

Structural Dynamics of DNA-Associated Chaperon Facilitates Chromatine Transcription

Olesya Volokh¹, Anastasia Sivkina¹, Maria Karlova¹, Elena Kotova², Vasily Studitsky^{1,2}, Olga Sokolova¹

¹*Biology Faculty, Lomonosov Moscow State University, Moscow, Russia*

²*Fox Chase Cancer Center, Philadelphia, Pennsylvania, USA*

Background: Histone chaperon FACT (“FACilitates Chromatin Transcription”) is a multifunctional and conserved eukaryotic protein involved in DNA transcription, replication and repair; which can reversibly unfold nucleosomes in presence of ATP. FACT is necessary for the viability and growth of breast tumor cells meanwhile in normal cells it can be knocked out without loss of vitality. Human FACT (hFACT) is a target for promising anticancer drug curaxins, which causes FACT trapping in chromatin of cancer cells and destabilizes the nucleosome. The nucleosome-unfolding activity is an important function of hFACT *in vivo*; however, the mechanism of FACT-dependent nucleosome unfolding remains unknown.

Methods: Here, we studied negative stained hFACT structure using single particle electron microscopy using JEOL 2100 TEM. Micrographs were captured with 25k magnification, and 4.1 Å pixel size. EM images pre-processing and single particles collection were performed in EMAN2.3, followed by 2D-particles analysis in RELION2.0. Final 2D-classes included ~70 000 single particles images.

Results: Based on 2D-classes data analysis we evaluated several states of hFACT reflecting its conformational flexibility: the “closed” complex is characterized by four domains localized close to each other and forming a compact structure; “intermediate” state represented by classes with identified three domains having compact structure and more disordered fourth domain, and the “open” complex, represented by three domains forming almost linear structure. The “closed” and “open” states are present in comparable amounts and significantly outnumber the “intermediate” state. It has been shown that hFACT domains are connected through flexible linkers and SPT16 and SSRP1 dimerization domains (DDs) form the “joint”-like connection between the two subunits. In the “closed” conformation, the DNA-binding surface of FACT is covered by its two C-terminal and middle domains (MDs). The N-terminal domain (NTD) of SPT16 was not resolved previously, but it is the best candidate for the forth domain that is clearly visible only in the “closed” conformation of hFACT, based on its dimensions and the longest linker length.

Conclusion: We propose that during conversion to the “open” complexes SPT16 NTD is moving away from the other subunits leading to formation of the first intermediate state with the NTD domain poorly resolved or not resolved, while less mobile DDs and MDs maintain more compact structure and the DNA-binding site is still protected by the CTDs. In the “open” state SPT16/SSRP1 visible MDs and DDs form almost linear

structure, unmasking the DNA-binding sites and making them accessible for the interaction with a nucleosome.

Key Words: transcription, nucleosome, FACT

This work was supported by the Russian Science Foundation (Grant No. 19-74-30003). Electron microscopy was performed on Unique scientific installation ‘3D-EMC’.

***Corresponding author:** Olesya Volokh. E-mail: olesyavolokh@gmail.com

P-29

http://dx.doi.org/10.21103/IJBM.11.Suppl_1.P29

Cryoem Study of the Inhibition of Bacterial Ribosomes by Madumycin II

Alena Yakusheva^{1,2}, Olga Shulenina^{1,2}, Evgeny Pichkur^{1,2}, Alena Paleskava^{1,3}, Alexander Myasnikov^{1,4}, Andrey Konevega^{1,2,3}

¹*Petersburg Nuclear Physics Institute - NRC KI, Gatchina, Russia*

²*NRC “Kurchatov Institute,” Moscow, Russia*

³*Peter the Great St.-Petersburg Polytechnic University, St. Petersburg, Russia*

⁴*Dubochet Center for Imaging (DCI) at EPFL, Lausanne, Switzerland*

Background: The efficiency of widely used antibiotics is limited by continuous improvement of resistance mechanisms. Thus, the research of poorly studied drugs that have not received practical use until now becomes relevant again. Protein translation is one of the major targets for antibiotics. Madumycin II (MADU) is an antibiotic of the streptogramin A class that binds to the peptidyl transferase center of the initiated bacterial 70S ribosome inhibiting the first cycle of peptide bond formation (I.A. Osterman et al. *Nucleic Acids Res.*, 2017). The ability of MADU to interfere with translating ribosome is an open question that we address by investigation of high-resolution cryo-EM structures of MADU bound 70S ribosome complexes from *Escherichia coli*.

Methods: Purified initiated and translating ribosome complexes preincubated with MADU were applied onto freshly glow discharged carbon-coated grids (Quantifoil R 1.2/1.3) and flash-frozen in the liquid ethane pre-cooled by liquid nitrogen in the Vitrobot Mark IV. Frozen grids were transferred into an in-house Titan Krios microscope. Data were collected using EPU software. Movie stacks were preprocessed in Warp software. For image processing, we have used several software packages: Relion 3.1, CryoSPARC, and CistEM. The model was built in Coot.

Results: We have obtained high-resolution cryo-EM structures of two ribosomal complexes with MADU before and after the first cycle of peptide bond formation with an average resolution of 2.3 Å. Preliminary analysis of the structures shows no major differences in the MADU binding mode to the ribosomal complexes under study suggesting that the quantity of amino acid residues attached to the P-site tRNA does not impact MADU bonding. Moreover, in both cases, we observed similar destabilization of the CCA-ends of A- and P-site tRNAs underlining the comparable influence of MADU on the ribosomal complexes.

Conclusion: Our results suggest that although MADU binding site is located in the peptidyl transferase center, the presence of the second amino acid residue on the P-site tRNA does not preclude antibiotic binding. We assume that further elongation of the polypeptide chain would not have any impact

either. High conformational lability of the CCA-ends of tRNA at the A and P sites upon binding of MADU obviously plays an important role in the inhibition mechanism of the bacterial ribosome. The further structural and biochemical analysis will be necessary to shed more light on the detailed mechanism of MADU action.

Key Words: ribosome, antibiotics, structure, cryo-EM

This work was supported by the Russian Science Foundation (Grant No. 17-14-01416)

***Corresponding author:** Alena Yakusheva. E-mail: yakusheva_av@pnpi.nrcki.ru

P-30

http://dx.doi.org/10.21103/IJBM.11.Suppl_1.P30

Structure of the 80S Ribosome from *Candida Albicans* Revealed by Integrative Structural Biology Approach

Yuriy Zgadzay^{1,2}, Olga Kolosova², Artem Stetsenko³,
Konstantin Usachev¹, Shamil Validov¹, Albert Guskov^{3,4},
Marat Yusupov^{1,2}

¹Laboratory of Structural Biology, Institute of Fundamental Medicine and Biology, Kazan Federal University, Kazan, Russia

²Department of Integrated Structural Biology, Institute of Genetics and Molecular and Cellular Biology, University of Strasbourg, Illkirch, France

³Groningen Biomolecular Sciences and Biotechnology Institute (GBB), University of Groningen, Groningen, the Netherlands

⁴Moscow Institute of Physics and Technology, Dolgoprudny, Russia

Background: The fungus *Candida albicans* is one of the most common fungal human pathogens, causing numerous mucocutaneous infections. About 80% of the world population is colonized with this pathogen, and in many cases, it does not reveal its pathogenic properties. However in the events when the suppression of normal bacterial flora occurs, e.g. as a consequence of chemotherapy or antibiotics treatment, multi-resistant strains of *Candida albicans* can rapidly colonize the host organism and prevent the normal flora recovery, which in turn can trigger many other diseases especially in the case of immunocompromised patients.

Methods: We used an integrated structural biology approach based on the single-particle cryo-EM reconstruction and macromolecule X-ray crystallography.

Results: One of the most promising targets for antibiotic action is a protein synthesis apparatus and ribosomes in the cell. In this study, we characterized structurally the protein synthesis machinery of *Candida albicans* using the state-of-the-art techniques of single-particle Cryo-electron microscopy and macromolecular X-ray crystallography.

Conclusion: We obtained the 2.4 Å resolution structure of the 80S ribosome from *Candida albicans* and the 4.2 Å resolution structure of the vacant *C. albicans* ribosome by X-ray crystallography. We believe that this study will shed light on mechanisms of antimicrobial resistance in *C. albicans* and improve candidiasis treatment in the future.

Key Words: ribosome, *Candida albicans*, X-ray crystallography, cryo-electron microscopy

This work was supported by the Russian Science Foundation (Grant No. 20-65-47031)

***Corresponding author:** Konstantin Usachev. E-mail: k.usachev@mail.ru

EM RESEARCH RELATED TO MEDICINE

P-31

http://dx.doi.org/10.21103/IJBM.11.Suppl_1.P31

Assembly of the Complex of the 30S Ribosomal Subunit and the Ribosome Maturation Factor P from *Staphylococcus aureus* for Structural Studies by Cryo-Electron Microscopy

Natalia Garaeva¹, Aydar Bikmullin¹, Evelina Klochkova¹, Shamil Validov¹, Marat Yusupov^{1,2}, Konstantin Usachev¹

¹Institute of Fundamental Medicine and Biology, Kazan Federal University, Kazan, Russia

²Institut de Génétique et de Biologie Moléculaire et Cellulaire, Université de Strasbourg, Illkirch, France

Background: *Staphylococcus aureus* (*S. aureus*) is one of the main human pathogens causing numerous nosocomial soft tissue infections and is among the best-known causes of bacterial infections. The bacterial 70S ribosome consists of two subunits, designated the 30S (small) and 50S (large) subunits. The small subunit (30S) consists of 16S ribosomal RNA (rRNA), from which the assembly of 30S begins, and 21 ribosomal proteins (r-proteins). The ribosome maturation factor P (RimP protein) binds to the free 30S subunit. Strains lacking RimP accumulate immature 16S rRNA, and fewer polysomes and an increased amount of unassociated 30S and 50S subunits compared to wild-type strains are observed in the ribosomal profile. Structural studies of the 30S subunit complex and the ribosome maturation factor RimP will make it possible in the future to develop an antibiotic that slows down or completely stops the translation of *Staphylococcus aureus*, which will complicate the synthesis and isolation of its pathogenic factors. Here we present the protocol of the *in vitro* reconstruction of *S. aureus* 30S ribosome subunit in a complex with RimP for further structural studies by cryo-electron microscopy.

Methods: Recombinant RimP protein from *S. aureus* was expressed in *E. coli* and purified by Ni-NTA chromatography and size exclusion chromatography. Reconstitution of the 30S–RimP complex was performed by mixing RimP protein with 30S ribosome. Unbound RimP protein was removed by Amicon Ultra Concentration (Merk KGaA, Darmstadt, Germany) with a cut-off limit of 100 kDa. The presence of RimP protein in the resulting 30S–RimP complex was confirmed by SDS-PAGE, and the quality of the final sample was analyzed by the negative staining EM.

Results: Finally, by *in vitro* reconstruction, the 30S–RimP complex from *S. aureus* was obtained for further structural studies by cryo-electron microscopy.

Key Words: ribosome, cryo-electron microscopy, ribosome maturation factor

This work was supported by the Russian Foundation for Basic Research (project № 20-34-70021)

***Corresponding author:** Konstantin Usachev. E-mail: k.usachev@mail.ru

P-32

http://dx.doi.org/10.21103/IJBM.11.Suppl_1.P32

Lung Structural Changes in COVID-19 Patients

Valery P. Kartashev¹, Djамshid N. Mardonov²,
Bahshillo R. Mamirov³, Azamat Kh. Butaev³

¹Russian State Social University, Moscow, Russia

²Republican Specialized Scientific Practical Medical Center of Surgery named after acad. V.Vakhidov, Tashkent, Uzbekistan

³First Zangiota Specialized Infectious Diseases Hospital, Tashkent, Uzbekistan

Background: The main causes of death from COVID-19 are lung lesions with the development of respiratory failure. However, structural changes in the lung tissue in this pathology are poorly studied. We examined autopsy material from patients with COVID-19.

The severe condition of patients, the manifestation of pulmonary symptoms of damage (cough, dyspnea) and the high probability of viral pneumonia at COVID-19 led to the widespread use of CT diagnostics in this group of patients, which allowed to identify of the primary signs of the disease, their subsequent transformation as well as the most adverse radiation symptoms corresponding to the severe course of the process (Speranskaya, 2020; Pan et al., 2019).

In the cases studied by us, the detection of typical symptoms revealed by radiation diagnostics of COVID-19 was subsequently confirmed by PCR data, which may indicate a high information content and specificity of detecting CT symptoms of a lesion as a method of primary diagnostics.

The aim of our study is to confirm at the microscopic level the correspondence of MSCT changes.

Methods: The material was taken at autopsy of deceased patients, fixed in 10% formalin solution in phosphate buffer, paraffin sections were stained with hematoxylin and eosin. The autopsy material was examined using a Carl Zeiss light microscope, Axioskop 40.

Results: Studies have shown that most of the alveoli of the lung tissue kept their airiness. However, their lumens were significantly reduced due to a significant thickening of the interalveolar septa caused by pronounced inflammatory infiltration mainly by lymphocytes. The most significant changes were revealed from the side of the microvasculature. There are numerous blood clots of various sizes in the lumen of most micro-vessels. The walls of microvessels have been significantly thickened with pronounced inflammatory infiltration and significant edema. The lumens of microvessels have been characterized by significant polymorphism. Intraluminal clots have been also characterized by pronounced polymorphism. The parietal pleura has been thickened. This has been reflected in the MSCT images and corresponds to the processes of perivascular infiltration.

Conclusion: The primary CT pattern of COVID-19 is a picture of infiltration of individual secondary pulmonary lobules of the "ground glass" type, followed by a decrease in the lesion volume at a favorable course of the disease, or their increase, the addition of a CT picture of a "cobblestone pavement" and the appearance of alveolar infiltration in the area of "ground glass" at the unfavorable course of the disease.

Key Words: COVID-19, pneumonia, lymphocytes, microvessels

***Corresponding author:** Valery Kartashev. E-mail: kvpmos@mail.ru

P-33

http://dx.doi.org/10.21103/IJBM.11.Suppl_1.P33

Structural Basis for the Growing Microtubule End Recognition by End Binding Proteins

Alena V. Korshunova

Center for Theoretical Problems of Physicochemical Pharmacology, Russian Academy of Sciences, Moscow, Russia

Background: Eukaryotic end binding proteins (EBs) can follow the growing microtubule end. EBs play a crucial role in microtubule dynamic instability and promote simultaneously growth rate and catastrophe frequency. It makes EB-like proteins perspective drug targets for a wide number of diseases. But the molecular mechanism of tip tracking by EB-like proteins remains unknown. Studies of mutants have revealed that the conservative amino acid Q102 (numbering relative to the human EB1 protein) plays a key role in the recognition of the growing microtubule end. However, the 3D structure studies revealed that this amino acid has no bonds with tubulin. In this work, we performed structural and phylogenetic analysis of EBs proteins to identify a possible molecular mechanism behind the plus end tracking.

Methods: UCSF Chimera10 was used for structural analysis. Phylogenetic analysis was performed with MEGA X software. 3D structures of EBs and microtubules with different states of GTP hydrolysis were used (pdb 3JAK, 3JAS, 3JAT, 3JAW, 3JAL, 3JAR, 6DPU, 6DPV, 6DPW).

Results: We have shown that two conservative amino acids (K100, E106) should play an important role in the recognition of the microtubule plus end in addition to Q102. It was concluded that these amino acids together form the plus-end «navigation site» of EBs. Analysis of possible interaction of the «navigation site» amino acids with microtubules in different conformational states suggested that the main mechanism of growing microtubule end recognition is not due to an affinity increase for a certain state of tubulin in microtubules at their end, but it due to a significant affinity decrease in other parts of the microtubule as a result of steric clashes.

Conclusion: Thus, the results of the analysis suggested the possible molecular mechanism that provides the tip tracking by EB-like proteins and allowed us to identify the key amino acids of this mechanism.

Key Words: microtubule, phylogenetic analysis, structure

This work was supported by the Russian Foundation for Basic Research (Grant No. 20-34-70159)

***Corresponding author:** Alena Korshunova. E-mail: korshunova.av@gmail.com

P-34

http://dx.doi.org/10.21103/IJBM.11.Suppl_1.P34

Cryo-EM Study of Submicrocapsules with a Shell of Nanoparticle Heteroaggregates and Polyelectrolyte Layers

Anastasiya Kostenko¹, Konstantin Palamarchuk¹, Yury Chesnokov¹, Konstantin Plokhikh¹, Tatyana Bukreeva^{1,2}, Roman Kamyshinsky^{1,2}

¹National Research Centre "Kurchatov Institute," Moscow, Russia

²Shubnikov Institute of Crystallography of FSRC "Crystallography and Photonics" RAS, Moscow, Russia

Background: Currently, different approaches of active and passive targeted drug delivery are being developed. One of the most promising methods of targeted drug delivery is the use of capsules. For instance, colloidosomes—capsules consisting of the shell formed by colloidal particles at the interface of the emulsion—can be used for targeted delivery of antitumor drugs

or any other drugs in liquid form. Here we present results of cryo-EM study of submicrocapsules with the soybean oil core and with the shell consisting of SiO₂ nanoparticles and detonation nanodiamonds (DNDs) stabilized with chitosan and alginate.

Methods: Cryo-electron tomography (Cryo-ET) was used to identify the morphological features of the submicrocapsules. Preliminary screening of samples and cryo-ET data collection were performed using Titan Krios cryo-EM (ThermoFisher Scientific, US) equipped with Falcon 2 direct electron detector. The restoration of the tomographic series was carried out using IMOD software. Eman2 was used for segmentation and UCSF Chimera was used for visualization of the 3D model. Submicron capsules were obtained by stabilizing oil droplets with a mixture of SiO₂ nanoparticles and DNDs. To form a stable shell, an additional layer of silica particles and polyelectrolyte layers of alginate/chitosan were applied to the droplets of the dispersed phase of the emulsion by physical adsorption.

Results: Cryo-EM data showed the presence of submicrocapsules with a diameter in the range of 200-900 nm. Although a significant fraction of submicrocapsules was found to be partially destroyed, results of cryo-ET study of intact capsules demonstrated that silicon dioxide nanoparticles form a net, while DNDs form clusters.

Conclusion: Here we demonstrate the results of the study of submicron capsules with a shell of silica nanoparticles and DNDs. It was found that a uniform distribution of DNDs is not a prerequisite for the creation of submicron capsules that contradicts the theoretical model.

Key Words: submicrocapsules, cryo-EM, cryo-ET

This work was supported by the Russian Foundation for Basic Research (Grant No. 18-53-34007)

***Corresponding author:** Anastasiya Kostenko. E-mail: nas-kostenko@mail.ru

P-35

http://dx.doi.org/10.21103/IJBM.11.Suppl_1.P35

Cryo-Electron Tomography of Protein Conjugated Upconverting Nanophosphors

Vyacheslav A. Kralin¹, Anton S. Orekhov^{1,2}, Roman A. Kamyshinsky^{1,2}, Yury M. Chesnokov², Polina A. Demina³

¹Institute of Physics and Technology, Moscow, Russia

²National Research Centre "Kurchatov Institute," Moscow, Russia

³Shemyakin-Ovchinnikov Institute of Bioorganic Chemistry, RAS, Moscow, Russia

Background: Over the past decades, significant advances have been made in the field of creating nanobioreagents for solving modern medicine problems (Greibenik et al., JBO, 2013). However, the problem of their low accumulation rate in pathological tissue in vivo experiments still remains. First of all, it is associated with the adsorption of blood proteins on the surface of nanobioreagents and the protein layer formation, which significantly changes the surface properties, which leads to their rapid excretion by the reticuloendothelial system. In particular, it is possible to reduce the blood plasma proteins adsorption and increase the time spent in the circulatory system by forming a coating of proteins.

Methods: In situ cryoelectron tomography (Cryo-ET) is the only method that allows the experimental observation of protein structures on the nanoparticle's surface in their natural functional state. The basic principle of the method is to obtain a series of projections of a vitrified sample thin lamella

at different tilt angles related to an incident electron beam. Their further processing leads to obtaining the volumetric information about the structure of the sample. The use of a cryo-focused ion beam (Cryo-FIB) in specimen thinning makes it possible to carry out experiments with thin sections of cellular structures and observe the penetration of nanoparticles into the intracellular environment.

Results: Upconverting nanophosphors (AN) were used as a nanopatform for creating a protein coating. To create a protein coating on the AN surface, they were functionalized using an amphiphilic polymer containing carboxyl groups. Then, conjugation with protein molecules from the class of immunoglobulins was carried out by the method of carbodiimide activation.

At each stage of synthesis and modification, AN solutions with different size distribution were vitrified for subsequent tomography. After a series of experiments to study the morphology of nanoparticles, an experiment on their successful absorption by cells of the cancer line A549 was carried out.

Conclusion: Within this work, a series of in situ Cryo-ET methods were proposed and applied for structural characterization and visualization of the processes of synthesis, modification, and engulfment of nanoparticles into cellular systems. For the first time in its native form, the engulfment of ANF into the internal environment of the A549 cancer line cells was demonstrated.

Key Words: cryo-tomography, upconverting nanophosphors

This work was financially supported by the National Research Center "Kurchatov Institute" (order dated 02.07.2020 No. 1056)

***Corresponding author:** Vyacheslav Kralin. E-mail: kralin.va@phystech.edu

P-36

http://dx.doi.org/10.21103/IJBM.11.Suppl_1.P36

Structural Analysis of Conformational Changes of Bacterial and Eukaryotic Tubulins

Liubov O. Makarova^{1,2}, Alena V. Korshunova³

¹Moscow Institute of Physics and Technology, Dolgoprudny, Russia

²Physics Department, Lomonosov Moscow State University, Moscow, Russia

³Center for Theoretical Problems of Physicochemical Pharmacology, Russian Academy of Sciences, Moscow, Russia

Background: Eukaryotic α - and β -tubulin proteins stand out among tubulin-like proteins by their ability to form hollow dynamically unstable microtubules (MT) with 13 protofilaments. Microtubules are part of the cell cytoskeleton and play a key role in chromosome division in mitosis. A considerable amount of anticancer drugs works on microtubules level breaking its dynamic. But the mechanism of dynamic instability and works of these drugs remains unknown. Bacteria of the genus *Prostecobacter* have unique bacterial tubulins (BtubA/B) capable to form hollow dynamically unstable 5 protofilament MTs (miniMT). Instead of great differences, both tubulins have many common features. Eukaryotic tubulin was known to have structural changes through GTP hydrolysis (compactization for approximately 2 Å and a twist for 0,1°). «Anchor point» structure in alpha-tubulin was noticed to be a fixed point in this movement.

Methods: We performed comparative structural analysis of BtubA/B and α - and β -tubulin proteins using USCF Chimera10 and MEGA X software. This data was obtained due to a comparison of 3 structures of microtubules with different

nucleotides [pdb6DPU, 6DPV, 6DPW] and two structures for bacterial tubulins (miniMT [pdb5o09] and BtubA/B-dimer [pdb2BTQ]).

Results: We noticed that bacterial tubulins form shorter protofilaments in miniMT than eukaryotic ones. It can be explained as compaction in two sites instead of one site in eukaryotic MT. Also, the most motionless point of mini MT turned out the same "anchor point." Phylogenetic analysis showed that this structure is very conservative in these orthologs. Moreover, the final state of both tubulins (GDP) repeats each other.

Conclusions: Our results suggest that bacterial tubulin can have movements through GTP hydrolysis similar to eukaryotic one. And it means that despite different amino acid sequences, bacterial and eukaryotic tubulins have similar keys structures for dynamic instability.

Key Words: α -tubulin, β -tubulin, Prostecobacter, structure
This work was supported by the Russian Foundation for Basic Research (Grant No. 20-34-70159)

*Corresponding author: Liubov Makarova. E-mail: makarova.lo@phystech.edu

P-37

http://dx.doi.org/10.21103/IJBM.11.Suppl_1.P37

Phosphorous Mapping in Inactivated SARS-CoV-2 Particles by Electron Energy Loss Spectroscopy

Andrey Moiseenko¹, Lubov Kozlovskaya^{3,4},
Aydar Ishmukhametov^{3,4}, Alexey Egorov^{1,2},

Konstantin Shaitan^{1,2}, Mikhail Kirpichnikov¹, Olga Sokolova¹

¹Lomonosov Moscow State University, Moscow, Russia

²N.N.Semenov Federal Research Center for Chemical Physics, Russian Academy of Sciences, Moscow, Russia

³Chumakov Federal Scientific Center Research and Development of Immune and Biological Product of Russian Academy of Sciences, Moscow, Russia

Background: The severe COVID-19 pandemic started in December 2019 is caused by the SARS-CoV-2 virus. The SARS-CoV-2 virion consists of a positive-sense single-stranded RNA (ssRNA), bound with the nucleocapsid N protein and surrounded by a lipid membrane with the embedded glycoprotein S and the transmembrane proteins M and E. The structure of inactivated SARS-CoV-2 virions is crucial for the development of vaccine-induced immunity. Here we characterized the nucleic acid distribution within β -propiolactone inactivated whole-virion SARS-CoV-2 vaccine CoviVac.

Methods: We used EELS to verify the presence of phosphorus (P) inside the β -propiolactone inactivated virions. Electron microscopy was performed with a JEM-2100 200kV LaB6 transmission electron microscope (JEOL, Japan) equipped with a Gatan GIF Quantum ER energy filter (Gatan, USA) operating in spectrometer mode, along with a High-Angle Annular Dark-Field (HAADF) scanning transmission electron microscopy (STEM) detector. The cooling holder model 21090 (JEOL, Japan) was operated at -182 °C to reduce the contamination effects and to enhance the specimen's stability under the electron beam. We employ a negative stain with 2% (NH₄)₂MoO₄ rather than uranyl acetate since the Uranium O_{4,5} peak (edge at 96 eV) is close to the P L_{2,3} peak (edge at 132 eV) and interferes with the accurate background interpolation.

Results: The intensity under the P peak after the background subtraction was used for STEM-EELS mapping. We observed the characteristic P signal from the inner part of the virion but not from the bare grid. The observed P signal could arise from either viral RNA or lipids of the virus membrane, and since the P signal is highly heterogeneous, it is more likely to originate from RNA.

Conclusion: So far, phosphorous mapping in individual virions using EELS was done only with samples prepared using highly specialized techniques, which minimized the sample thickness, including the substrate thickness. Here, we performed elemental mapping on ordinary samples of whole viruses. All investigated virions contained P signal, but its spatial distribution and intensity differed significantly. This clearly reflects the non-even distribution of the genomic RNA, which, apparently, accompanies their inner heterogeneity, previously observed by in situ cryo-electron tomography.

Key Words: COVID-19, β -propiolactone inactivated virus particles, EELS, nucleocapsid.

This work was supported by the Russian Foundation for Basic Research (Grant No. 20-04-60258)

*Corresponding author: Andrey Moiseenko. E-mail: postmoiseenko@gmail.com

P-38

http://dx.doi.org/10.21103/IJBM.11.Suppl_1.P38

Tunable Soft Networks of Wormlike Micelles and Clay Particles

Vyacheslav S. Molchanov¹, Anton S. Orekhov^{2,3},

Natalia A. Arkharova⁴, Alexandr I. Kuklin⁵, Andrey V. Rogachev⁵,
Olga E. Philippova¹

¹Department of Physics, Lomonosov Moscow State University, Moscow, Russia

²National Research Centre "Kurchatov Institute," Moscow, Russia

³Moscow Institute of Physics and Technology, Dolgoprudny, Russia

⁴FSRC "Crystallography and Photonics" RAS, Moscow, Russia

⁵Joint Institute for Nuclear Research, Dubna, Russia

Background: Over the past few decades, there has been a great deal of interest in the aqueous self-assembly of surfactant molecules into giant wormlike micelles (WLMs). These cylindrical aggregates undergo reversible breakdown processes and in favorable cases can grow up to few tens of micrometers that is comparable with the length of high molecular weight polymer. The viscoelastic properties of WLMs can be easily modified by different additives like salts or polymers. A new emerging research area consists of tuning the WLM solution properties by inorganic nanoparticles. It suggests, in particular, the use of networks of entangled WLMs as a matrix for producing soft nanocomposites with different kinds of embedded nanoparticles that are promising for controlled release, template synthesis, and oilfield applications. These materials can combine adaptive rheological properties of the WLM matrix and the functionality of nanofiller.

Methods: Rheometry and cryo-transmission electron microscopy were combined to investigate the structure and properties of mixed WLMs of zwitterionic oleylamidopropyl dimethyl betaine and anionic sodium dodecyl sulfate surfactants and platelike particles of bentonite clay.

Results: This system demonstrates the formation of giant linear long-lived WLMs, which even at extremely low surfactant concentrations reach a sufficient length to entangle with each other and form a temporally persistent network. The

stability of these micelles can be due to electrostatic attraction between the headgroups of the anionic and zwitterionic surfactants and favorable volume/length hydrophobic ratio in the surfactant mixture. At increasing surfactant concentration, the long-lived linear micelles transform into fast-breaking branched micelles.

Stable viscoelastic suspensions of clay particles in semi-dilute solutions of WLM were elaborated. They represent a novel type of soft nanocomposite with the tunable matrix. Structural studies revealed that the clay is dispersed in a dense network of entangled WLM in the form of 100-nm tactoids. Rheological investigations demonstrated that clay particles can induce an increase of viscosity and relaxation time by up to one order of magnitude. The effect of the clay becomes more pronounced with increasing content of anionic surfactant, when the micelles become branched. This behavior was explained by the stabilization of micelle-nanoclay junction points due to the screening of the repulsion between positively charged fragments of zwitterionic head groups by added anionic surfactant.

Conclusion: The pronounced effect of nanoparticles on the viscoelasticity of the network formed by branched WLMs was observed for the first time. The nanoparticles-WLM junctions were confirmed by cryo-TEM data. The elaborated systems are of interest for many industrial applications.

Key Words: Wormlike micelles, clay nanoparticles, zwitterionic surfactant

This work was supported by the Russian Science Foundation (project № 17-13-01535)

***Corresponding author:** Vyacheslav Molchanov. E-mail: molchan@polly.phys.msu.ru

P-39

http://dx.doi.org/10.21103/IJBM.11.Suppl_1.P39

Fluorescent Silver Nanoclusters with Immunoglobulins and Albumins

Olga V. Morozova, Nataliya V. Shevlyagina, Vladimir G. Zhukhovitsky

National Research Center of Epidemiology and Microbiology of N.F. Gamaleya of the Russian Ministry of Health, Moscow, Russia

Background: Multiplex biomedical assays including molecular genetic tests and immunoanalysis require multiple fluorophores with a wide excitation range and different emission spectra. In comparison with organic fluorophores and quantum dots, the metal nanoclusters (NC) consisting of a few to hundred atoms have the following advantages: small size, large Stokes shift, prolonged fluorescence lifetime and biocompatibility. Our research was aimed at construction of fluorescent AgNC with the main blood proteins and transmission electron microscopy (TEM).

Methods: AgNC were synthesized from AgNO₃ in the presence of albumins and immunoglobulins (Ig) of different classes and origin at pH 9-11 with NaBH₄ recovery. The resulting AgNC with proteins were loaded to "Formvar/Carbon 200 Mesh Copper" copper grids (Ted Pella, USA) and examined using TEM system JEM 2100 Plus (JEOL, Japan) without contrast. Fluorescence excitation/emission spectra were measured in quartz cuvette using the FluoroMax + spectrofluorometer (Horiba Scientific, Japan).

Results: Recovery of Ag⁺ ions did not occur in the presence of IgG and albumins without NaBH₄ at different temperatures, pH, and incubation time. Broad excitation spectra of AgNC were in

a range 340-540 nm. Their emission spectra correlated with the original AgNO₃ concentration and did not depend on protein and pH. NC stabilized with IgG or albumin with blue fluorescence and emission maximum at 420 nm contained NC from 0.6 nm and higher. Green AgNC with proteins had bright fluorescence at 430-470 nm and red NC showed emission maximum at 650 nm. TEM revealed discrete AgNC and their numerous aggregates in each sample of fluorescent NC in spite of different fluorescent emission spectra.

According to the MTT test, AgNC with human IgG and BSA with protein concentrations up to 3 mg/ml were not toxic for human larynx carcinoma HEP-2 cells despite cytotoxicity of silver nanoparticles covered with IgG or albumin envelopes as well as Cd and AuNC with BSA.

Conclusion: AgNC with antibodies and albumin with a broad size range and aggregation possess tunable fluorescence emission spectra with broad excitation at 340-540 nm. Different emission spectra permit AgNC to be used in multiplex assays. AgNC were not toxic for human tissue culture and may be applied for bioimaging.

Key Words: silver nanoclusters; fluorescent spectra; TEM; cytotoxicity.

***Corresponding author:** Olga V. Morozova. E-mail: omorozova2010@gmail.com

P-40

http://dx.doi.org/10.21103/IJBM.11.Suppl_1.P40

The Shape and Size of the Recombinant Virus-like Particles Were Checked by Means of Electron Microscope

Ivan Okhrimenko¹, Yulia Zagryadskaya¹, Alexey Tsarenko¹, Valentin Borshchevskiy¹, Andrey Rogachev¹, Marina Shevchenko²

¹Moscow Institute of Physics and Technology (MIPT), Dolgoprudny, Russia

²Shemyakin and Ovchinnikov Institute of Bioorganic Chemistry, Moscow, Russia

Background: Nucleocapsid protein of hepatitis-B virus (HBcAg) recombinantly synthesized in prokaryotic and eukaryotic cells is known to be capable to self-assemble into highly immunogenic stable viral-like particles (VLP) of icosahedral shape with a characteristic size of 32 nm (Schödel et al., 1994; Murray and Shiau, 1999). The VLP formation is tolerant to the insertion of some artificial epitopes to N- and C-termini of HBcAg monomer and also into major insertion region (MIR), forming a spike on the surface of VLP (Tordjeman et al., 1993; Peyret et al., 2015).

Methods: We have investigated the possibility of heterologous expression of *de novo* designed gene coding the first 148 amino acid residues of HBcAg (Pumpens and Grens, 1999). The gene was specially designed to be suitable for the insertions of genes coding fluorescent proteins, which are desired for the studies of VLP distribution in tissues by confocal microscopy. Gene was optimized for overexpression in *E. coli* producer strains and special attention was taken to obtain a simple purification scheme, which reliably reduces the amount of pyrogens in purified VLP.

The MIPT scientific platform of electron microscopy equipped with the transmission electron microscope Tecnai Polara G2 (Thermo Scientific (FEI)) was used. Carbon-coated (Lacey Carbon and 10 nm thin carbon) copper 200 mesh grids were treated with glow-discharge and coated with VLP suspension in deionized

water. The samples were stained with uranyl acetate solution, air-dried, and inspected at the accelerating voltage of 300 kV.

Results: The 32 nm size of heterologously synthesized VLP was successfully proved, and spherical shape was seen using negative contrasting.

Key Words: hepatitis-B virus, electron microscopy, VLP

This work was supported by the Russian Foundation for Basic Research (Grant No. 20-04-60311)

***Corresponding author:** Ivan Okhrimenko. E-mail: ivan.okhrimenko@phystech.edu

P-41

http://dx.doi.org/10.21103/IJBM.9.Suppl_1.P41

Contribution of Matrix-bound Vesicles Produced by Mesenchymal Stromal Cells in the Differentiation of Multipotent Stem Cells *in vitro*

Daria V. Selina¹, Ekaterina S. Novoseletskaia^{1,2}, Nataliya A. Basalova^{1,2}, Ilya V. Zubarev^{1,2}, Natalya A. Alexandrushkina^{1,2}, Andrey V. Moiseenko³, Olga S. Sokolova³, Anastasia Yu. Efimenko^{1,2}

¹*Institute for Regenerative Medicine, Medical Research and Education Center, Lomonosov Moscow State University, Moscow, Russia*

²*Faculty of Medicine, Lomonosov Moscow State University, Moscow, Russia*

³*Faculty of Biology, Lomonosov Moscow State University, Moscow, Russia*

Background: According to the current view on the extracellular matrix (ECM) composition and functions, it includes not only structural proteins and components of cell adhesion, but also various deposited components, including enzymes involved in ECM remodeling, growth factors, and matrix-bound vesicles (MBV). MBV can presumably participate in the formation of a specific microenvironment for stem cells and regulate their differentiation. However, the contribution of MBV to these processes remains poorly understood. In our work, we evaluated the effects of MBV within native ECM produced by mesenchymal stromal cells (MSCs) cultured in cell sheet on multipotent stem cell differentiation.

Methods: We isolated MBV from decellularized MSC-produced ECM by treatment with the following enzymes: collagenase, hyaluronidase, or trypsin, and centrifugation on 1000 kDa filters. The nanostructure and relative size in each sample were observed using TEM. The particle size and concentration were also studied with NTA. In addition, the obtained MBV were examined for the presence of key exosome markers using Western blot. Then we investigated the effect of MBV on the formation of capillary-like structures by endothelial cells (in vitro model of angiogenesis) as well as on the differentiation of primary MSCs isolated from human adipose tissue in the adipogenic, osteogenic, and chondrogenic directions.

Results: As a result of comparative analysis of isolation protocols, it was shown that all MBV samples had the characteristics of extracellular vesicles (EV), but differed in size and representation of exosomal markers. The MBV isolated from ECM did not stimulate the formation of capillary-like structures by endothelial cells, in contrast to EV secreted by MSCs to the conditioned medium, but maintained the viability of the endothelium. Isolated MBV stimulated osteogenic and adipogenic differentiation of MSCs similar to secreted EV. On the other hand, preincubation of MSCs with MBV leads to reorganization of

cell monolayer to spheroid-like structures during chondrogenic differentiation.

Conclusion: Here, we developed the protocol of isolation of MBV from ECM that have distinguished characteristics and functional activity.

Key Words: ECM; matrix-bound vesicles; differentiation; MSC

This work was supported by the Russian Foundation for Basic Research (Grant No.19-315-90060) and Russian Science Foundation (Grant No.19-75-30007)

***Corresponding author:** Daria Selina. E-mail: daria.selina13@gmail.com

P-42

http://dx.doi.org/10.21103/IJBM.11.Suppl_1.P42

Structure of Hydrogels of an Anionic Polysaccharide Studied by Freeze-Fracture Transmission Electron Microscopy

Andrey V. Shibaev¹, Maria E. Smirnova¹, Olga E. Philippova¹, Vladimir V. Matveev², Anatoly E. Chalykh²

¹*Department of Physics, Lomonosov Moscow State University, Moscow, Russia*

²*Frumkin Institute of Physical Chemistry and Electrochemistry, RAS, Moscow, Russia*

Background: Polysaccharide hydrogels draw attention due to the ability to form mechanically tough gels at low concentrations (typically 1 wt% or lower), combined with biocompatibility and biodegradability. Biopolymer hydrogels can be used as a matrix for cell growth, in order to obtain materials for the replacement of damaged tissues. “Physical” gels with macromolecules cross-linked by dynamic reversible cross-links are of great interest due to their self-healing ability. However, investigation of the native un-perturbed structure of such hydrogels presents a challenge, since they collapse upon drying, and present a difficulty for preparing a thin specimen for cryo-TEM experiments due to very high viscosity. The aim of this work is to study the native structure of hydrogels of an anionic polysaccharide – carboxymethyl hydroxypropyl guar (CMHPG) – cross-linked by borax..

Methods: Freeze-fracture transmission electron microscopy (FF-TEM) was conducted on a Phillips EM-301 microscope. A small volume of the sample (100 µl) was put into the copper cell and cooled down by liquid nitrogen, put under vacuum (10⁻⁵ torr) at continuous cooling with liquid nitrogen, and fractured. The surface was etched for 10–20 min at 10⁻⁵ torr and then replicated by spraying platinum and carbon.

Results: The gels have a microphase-separated microstructure – a rather thick (several nm) polymer backbone is seen, which is presumably formed by multiple aggregated macromolecules, and meshes between the backbone do not contain polymer and are filled with solvent. Mesh size determined from the micrographs qualitatively coincides with the value determined from the elastic modulus of the gels. Upon increasing the concentrations of cross-linker, the network becomes denser: the mesh size becomes lower, and the thickness of the backbone increases. Thus, the addition of cross-linker favors the aggregation of polymer chains forming the backbone.

Conclusion: It was shown by FF-TEM that cross-linked CMHPG gels have a microphase-separated structure with a dense backbone formed by polymer chains and rather large meshes between them.

Key Words: polysaccharide, hydrogel, guar, FF-TEM

This work was supported by the Russian Science Foundation (Grant No. 18-73-10162)

*Corresponding author: Andrey Shibaev. E-mail: shibaev@poly.phys.msu.ru

P-43

http://dx.doi.org/10.21103/IJBM.11.Suppl_1.P43

Effect of Glucocerebrosidase Dysfunction on the Pool of Plasma Exosomes of Patients with Gaucher Disease

Luiza A. Garaeva^{1,2,3}, Roman A. Kamyshinsky^{1,4}, Darya G. Kulabukhova^{1,5}, Sergey B. Landa¹, Elena Yu. Varfolomeeva^{1,2}, Sofya N. Pchelina^{1,2,5}, Tatiana A. Shtam^{1,2,6}

¹Petersburg Nuclear Physics Institute Named by B.P. Konstantinov of National Research Centre "Kurchatov Institute," Gatchina, Russia

²National Research Centre "Kurchatov Institute," Moscow, Russia

³Peter the Great St.Petersburg Polytechnic University, St. Petersburg, Russia

⁴Shubnikov Institute of Crystallography of FSRC "Crystallography and Photonics" RAS, Moscow, Russia

⁵First Pavlov State Medical University of St. Petersburg, St. Petersburg, Russia

⁶Institute of Cytology of Russian Academy of Sciences, St. Petersburg, Russia

Background: Extracellular vesicles (EVs) are small membrane vesicles released from different types of cells. EVs are found in many human biological fluids. Exosomes are a subtype of EVs that are released by the fusion of multivesicular bodies with the plasma membrane. This type of vesicles is characterized by specific exosomal markers. Exosomes extracted from peripheral body liquids could have specific properties associated with different physiological conditions as well as human disorders, including neurodegenerative diseases.

Gaucher disease (GD) – is the most common form of lysosomal storage disorders caused by mutations in the glucocerebrosidase (*GBA*) gene. Lysosome functionality is critical for the regulation of extracellular vesicle secretion and content. In model animals, the inhibition of glucocerebrosidase has been shown to increase the secretion of extracellular vesicles in brain tissues. Amount evaluation of EVs and their size in the biological fluids of patients with GD has not been early performed; therefore, it is unknown whether lysosomal dysfunction found in GD patients influences the plasma pool of EVs. The aim of this study was to evaluate the amount of blood plasma EVs in patients with GD and their characterization for morphology and size.

Methods: EVs were isolated from the blood plasma of 8 GD patients and 8 controls by ultracentrifugation, and were characterized using cryo-electron microscopy (cryo-EM), nanoparticle tracking analysis (NTA), and dynamic light scattering (DLS). Also, the presence of exosomal markers CD9, CD63, CD81, and HSP70 was analyzed by flow cytometry and western blot.

Results: Here, it was first shown an increased proportion of exosome fraction in EVs from plasma of GD patients compared to controls by DLS and cryo-EM ($p < 0.001$) that was confirmed by mode size detected by NTA ($p < 0.02$). Moreover, an increased number of double and multilayer vesicles in plasma EVs from GD patients was demonstrated by cryo-EM. We also detected an increase in the expression of exosomal markers on the surface of vesicles from the blood plasma of patients with GD compared to controls.

Conclusion: Here, we firstly report that the exosomes obtained from the blood plasma of GD patients have a larger size and altered morphology. Thus, we have shown that lysosomal dysfunction in GD patients leads to a striking alteration of blood plasma extracellular vesicle pool.

Key Words: cryo-EM; extracellular vesicles; exosomes; Gaucher disease

This work was supported by the Russian Science Foundation (project 19-74-20146 for cryo-EM experiments and project 19-15-00315 for NTA, DLS, and flow cytometry experiment)

*Corresponding author: Tatiana A. Shtam. E-mail: Shtam_TA@pnpi.nrcki.ru

STRUCTURE OF VIRUSES AND CHAPERONINS

P-44

http://dx.doi.org/10.21103/IJBM.11.Suppl_1.P44

SARS-CoV-2 Inactivation by Ultraviolet Light Does Not Violate Virus Morphology, Antigenic and Immunogenic Properties

Evgeny Faizuloev¹, Anastasiia Gracheva¹, Ekaterina Korchevaya¹, Grigory Glukhov², Olga Sokolova², Roman Samoilkov¹, Vitaly Zverev¹

¹I.Mechnikov Research Institute of Vaccines and Sera, Moscow, Russia

²Lomonosov Moscow State University, Moscow, Russia

Background: Vaccination is the most effective tool for reducing the morbidity and mortality of COVID-19. Particular interest is the development of whole-virion inactivated vaccines, since such vaccines include a complete set of viral structural proteins. One of the requirements for the whole-virion vaccines is the guarantee of complete virus inactivation while maintaining the native conformation of protective antigens. The aim of this study is to evaluate the effect of ultraviolet (UV) treatment on the morphology, antigenic and immunogenic properties of the SARS-CoV-2.

Methods: SARS-CoV-2, strain "Dubrovka" (GenBank No.: MW514307.1), grown in Vero CCL81 cell culture (ATCC). Viral reproduction was monitored by real-time qRT-PCR, ELISA and virus titration in Vero cells. Virus was inactivated by treating with ultraviolet light for 5 minutes using a standard biosafety cabinet UV irradiator. Virus inactivation control was performed by three "blind" passages in Vero cells. Clarified viral material was concentrated on Amicon MWCO 100 kDa (Millipore) columns. Negatively stained with uranyl acetate viral preparation was examined by transmission electron microscopy (TEM). Mice were immunized with a UV-inactivated virus subcutaneously in two variants (5 animals per group) - with and without Freund's adjuvant, twice with an interval between immunizations of 2 weeks. The titer of virus-neutralizing antibodies in mouse sera was determined in Vero cell culture.

Results: Preparation of the SARS-CoV-2 coronavirus with a titer of 7.5 lg TCID₅₀/ml and concentration of viral RNA of 8.5 lg copies/ml was obtained in Vero cells. After UV-treatment the presence in the preparation of SARS-CoV-2 antigen was confirmed by ELISA with a set of COVID-19 convalescent sera. The particles with coronavirus morphodiagnostic signs were imaged by TEM - rounded shape with characteristic spikes of 12-15 nm on the envelope, the diameter of the virion was 90-110 nm.

Neutralizing antibodies were detected in the sera of all immunized mice, whereas in animals of the control group neutralizing antibodies were not detected. Neutralizing antibodies titer was significantly higher in animals immunized by a virus with Freund's adjuvant - on average 448, than without adjuvant - 64 ($p < 0.01$).

Conclusion: Treatment of SARS-CoV-2 by UV light completely inactivates its infectivity, while retaining the typical coronavirus virions morphology, antigenic properties, and ability to induce in mice a synthesis of neutralizing antibodies.

Key Words: SARS-CoV-2, UV inactivation, transmission electron microscopy, neutralizing antibodies

This work was supported by the Russian Foundation for Basic Research (Grant No. 20-04-60079)

***Corresponding author:** Evgeny B. Faizuloev. E-mail: faizuloev@mail.ru

P-45

http://dx.doi.org/10.21103/IJBM.11.Suppl_1.P45

Structure of the Bacteriophage AR9 *Bacillus Subtilis* Chaperonin According to Cryo-Electron Microscopy

Ekaterina S. Maslova¹, Evgeny B. Pichkur², Pavel I. Semenyuk¹, Lidia P. Kurochkina¹, Olga S. Sokolova¹

¹Lomonosov Moscow State University, Moscow, Russia
²NRC "Kurchatov Institute," Moscow, Russia

Background: Chaperonins are a family of molecular chaperones Hsp60 (heat shock proteins 60). GroEL is a bacterial chaperonin. It ensures the correct folding of proteins, using the energy of ATP hydrolysis. Three-dimensional reconstructions of its predicted orthologs were obtained and biochemically characterized in free and nucleotide-bound states for bacteriophages EL *Pseudomonas aeruginosa*, OBP *Pseudomonas fluorescens* (Kurochkina, L. P. et al., *Journal of virology*, 2012; Semenyuk, P. I. et al., *Biochemical Journal*, 2016; Stanishneva-Konovalova, T. B. et al., *Journal of Structural Biology*, 2020). Physicochemical studies were carried out for the bacteriophage AR9 *Bacillus Subtilis* and confirmed that the protein has chaperone activity and does not require co-chaperonin to function (Semenyuk P. I. et al., *International Journal of Biological Macromolecules*, 2020).

Methods: The recombinant chaperonin of the B. subtilis bacterial phage AR9 (gp228) was isolated and purified in a free state and vitrified in Vitrobot Mark IV. Data were collected using a Titan Krios cryo-TEM and processed in Warp, RELION and cryoSPARC software.

Results: The final structures of the chaperonin were reconstructed with a C1 and C7 symmetry at the resolution of 4.5 Å and 4.0 Å respectively. Significant heterogeneity of the apical domains was addressed further using 3D classification and symmetry expansion in RELION resulting in a set of classes reflecting the conformational transition of the subunits between different states. At least four different conformational states of the subunit were clearly resolved.

Conclusion: Gp228 structure show similarities between bacteriophage chaperonin and also bacterial chaperonin GroEL. It is formed by a single ring consisting of seven identical subunits, each has three domains: equatorial, intermediate, and apical. The subunits of the apo-form chaperonin Gp228 exhibit significant conformational flexibility in the apical and intermediate domains.

Key words: chaperonin, cryo-EM, structure

This work was supported by the Russian Foundation for Basic Research (Grant No. 19-04-00605 to O.S.S.). The authors acknowledge the Resource Center of Probe and Electron Microscopy at the NRC "Kurchatov Institute."

***Corresponding author:** Ekaterina S. Maslova. E-mail: ekatherine.ms@gmail.com

P-46

http://dx.doi.org/10.21103/IJBM.11.Suppl_1.P46

Structure of *A. baumannii* Phage Tapaz, Revealed with Cryoelectron Microscopy

Andrey V. Moiseenko¹, Yueqi Wang², Daniil Litvinov¹, Anastasia V. Popova^{3,4}, Mikhail M. Shneider⁴, Konstantin A. Miroshnikov⁴, Olga S. Sokolova^{1,2}

¹Lomonosov Moscow State University, Moscow, Russia

²MSU-BIT Shenzhen University, Shenzhen, China

³State Research Center for Applied Microbiology and Biotechnology, Obolensk, Russia

⁴Institute of Bioorganic Chemistry RAS, Moscow, Russia

Background: *Acinetobacter baumannii* is an opportunistic pathogen and one of the six most important multidrug resistant microorganisms in hospitals worldwide. Some of its strains are resistant to most of the antibiotics, *A. baumannii* is included into the Priority 1 part of Global Priority List of Antibiotic-resistant Bacteria. Phage therapy is considered to be an alternative strategy to antibiotic treatments.

Methods: *A. baumannii* strain NIPH601 cells were grown till OD6000.4 and infected with the phage at MOI 10:1. After complete lysis took place cell debris was spined down and phage particles were precipitated with the PEG6000 (final concentration 10% PEG 6000, 0.5 NaCl). Virus particles were collected by centrifugation, resuspended at SM buffer and applied on CsCl step gradient. Gradient was spined down for 2 hours at 40000g and the fraction containing phage particles was collected and dialyzed against SM buffer.

Purified phage particles were applied to Quantifoil 1.2/1.3 grids and plunge-froze in Vitrobot Mark IV (TFS) Micrographs were collected in HKU, Shenzhen campus with Titan Krios cryoelectron microscope (TFS), equipped with Gatan K3 direct electron detector. The micrographs were acquired with 1.06 Å pixel size and 1.5 μm average defocus value in counting mode with 50 frames and 1.2 e/Å²/frame dose rate. All image processing was performed with Relion3.0 software, except for the particle picking step performed with cryolo.

Results: Lytic *A. baumannii* phage TaPaz belongs to the family *Myoviridae*. BLAST search over NCBI "nr" (non-redundant) database revealed close homology with previously published sequences of *Acinetobacter* phage vB_AbaM_B9 and *Acinetobacter* phage BS46. However, no structural information about any homologous proteins was found among the PDB structures.

The cryo-EM map was reconstructed with single particle analysis independently for the capsid, tail and baseplate regions. The capsid was reconstructed at 3.9 Å resolution with I3 symmetry applied (Fig. 1A). The baseplate region of the phage was reconstructed at 3.5 Å resolution with C3 symmetry (Fig. 1B). The tail region was reconstructed at 2.6 Å resolution with helical symmetry (Rise 36.4 Å, Twist 25.7 deg). Initial atomic model for the tail region was built from sequence with DeepTracer and was further refined in coot (Fig. 1C).

Conclusion: We successfully obtained the near-atomic resolution structural map of phage TaPaz. The data obtained contribute to enhancing knowledge of structural diversity of bacterial viruses infecting *A. baumannii*.

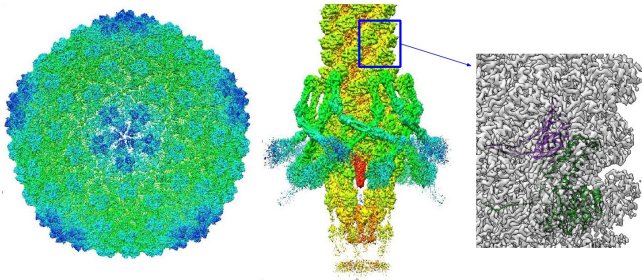


Fig. 1. (A) – Capsid and (B) baseplate cryo-EM maps, (C) – Tail sheath and tube asymmetric subunit cryo-EM map with atomic model

Key Words: cryo-EM; *A. baumannii*; phage TaPaz.

This work was supported by the Russian Foundation for Basic Research (19-04-00605 to O.S.S.). We thank Dr Zheng Liu from HKU for help with collecting the cryo-EM data.

***Corresponding author:** Andrey Moiseenko. E-mail: postmoiseenko@gmail.com

P-47

http://dx.doi.org/10.21103/IJBM.11.Suppl_1.P47

Analysis of Phosphorus Distribution in Giant Bacteriophage Capsid by Electron Energy Loss Spectroscopy

Tatiana Trifonova¹, Andrey Moiseenko^{1,2}, Olga Shaburova³, Maria Bourkaltseva³, Viktor Krylov³, Olga Sokolova¹

¹Lomonosov Moscow State University, Moscow, Russia

²Semenov Institute of Chemical Physics, Russian Academy of Sciences, Moscow, Russia

³I.I. Mechnikov Research Institute of Vaccines and Sera, Moscow, Russia

Background: We have recently developed a method to visualize the distribution of DNA in the cytoplasm of bacteria by analytical electron microscopy (EM), using the Phosphorus signal (dsDNA contains two phosphate groups per each nucleotide pair), that was detected and mapped onto the image of the cell (Danilova et al, 2020; Loiko et al, 2020). Here we applied this technique to study much smaller objects – the DNA packing inside bacteriophage heads. We studied phiEL, giant phiKZ-like bacteriophage of the Myoviridae family that infects *Pseudomonas aeruginosa* (Krylov et al, 2003). We have earlier demonstrated that this phage contains an ‘inner body’ inside its capsid, which is responsible for the specific DNA packing (Sokolova et al, 2014).

Methods: The phage propagation was performed as described before (Sokolova et al, 2014). A 3 ul sample of purified bacteriophage phiEL was applied to the glow-discharged carbon-coated copper grid and stained with freshly prepared ammonium Molybdate 2% aquatic solution for 30 sec. Grids were loaded into Gatan cooling holder and the temperature of the specimen was kept at -180°C.

EELS spectra and phosphorus elemental maps were obtained on JEOL2100 microscope, operating at 200 kV with the Gatan GIF Quantum ER spectrometer in STEM mode. Pixel size was set to 15-20 nm. STEM drift correction was applied after each 40-50 pixels. Each spectrum was obtained at a 6.0 mrad collection angle, 0.25 eV dispersion, and 132 eV energy shift. The spectra from different pixels were aligned to carbon K-edge.

Results: Phosphorus mapping inside and outside the bacteriophage capsid was performed (Fig. 1). Outside the capsid, the phosphorus signal was practically absent, which corresponds to the presence of DNA only inside the capsid. The distribution of phosphorus inside the capsid was uneven: the rectangular area in the middle of the capsid contained a weak signal, while a more intense signal was detected on the periphery. This can be explained by the presence of an ‘inner body’ inside (Fig. 1C).

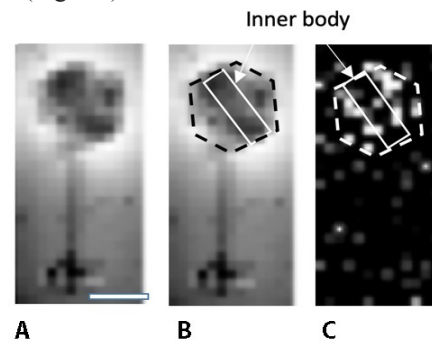


Fig. 1. Mapping of Phosphorus in bacteriophage EL. (A) HAADF image of phage EL. Bar – 100 nm; (B) the inner body (white rectangle, marked by the arrow) appears darker against the background of the DNA in the capsid (black dashes). (C) map of phosphorus distribution. The brightness of the pixels reflects phosphorus signal level.

Conclusion: Thus, our results justify the possibility of using the analytical EM technique to study the distribution of DNA by mapping Phosphorus in biological nano-objects at relatively low content of the element.

Key Words: analytical EM; EELS, *Pseudomonas aeruginosa*; phage phiEL, DNA packing.

This work was supported by the Russian Science Foundation (Grant No. 21-44-07002 to O.S.S.).

***Corresponding author:** Tatyana Trifonova. E-mail:trf@ya.ru

Author Index

- A**
 Armeev, Grigoriy A. P-1, P-5, P-19
 Azon, S. A. P-7
 Akhtar, Sohail P-18
 Afonina, Zhanna A. P-20, P-27
 Alexandrushkina, Natalya A. P-41
 Arkharova, Natalia A. P-38
- B**
 Bozdaganyan, Marine P-12, P-14
 Bikmullin, Aydar G. P-21, P-26, P-31
 Baymukhametov, Timur N. P-20, P-27
 Buyan, Andrey P-22
 Butaev, Azamat Kh. P-32
 Bukreeva, Tatyana P-34
 Basalova, Nataliya A. P-41
 Biňovský, Ján OR-6
 Buchta, David OR-7
 Borshechskiy, Valentin P-4, P-10, P-11, P-17, P-40
 Baranov, Mikhail P-10
 Bukhdruker, S. P-11
 Bourkaltseva, Maria P-47
 Belousov, Anatoly P-10
- C**
 Chesnokov, Yury OR-2, OR-2, P-3, P-15, P-34, P-35
 Chugunov, Anton O. OR-3
 Cherepanov, Peter OR-8
 Cherezov, Vadim P-4
 Chalykh, Anatoly E. P-42
- D**
 Dadinova, Liubov OR-2
 Dontsova, Olga A. OR-4
 Deyev, Igor P-13
 Dmitriev, Sergey E. P-22
 Demina, Polina A. P-35
- E**
 Egorov, Alexey M. OR-8, P-1, P-37
 Ezquerro, Artur OR-9
 Efimenko, Anastasia Yu. P-41
- F**
 Füzik, Tibor OR-7
 Fernandez-Leiro, Rafael OR-9
 Feofanov, Alexey V. P-9, P-24
 Fatkhullin, Bulat P-25
 Faizuloev, Evgeny P-44
- G**
 Gilep, A. P-11
 Garaeva, Luiza A. P-16, P-43
 Gensch, Thomas P-10, P-17
 Gerasimova, Nadezhda S. P-18, P-23, P-24
 Golubev, Alexander P-21, P-25
- Garaeva, Natalia P-21, P-26, P-31
 Geraskina, Olga P-24
 Guskov, Albert P-30
 Gracheva, Anastasiia P-44
 Glukhov, Grigory P-44
 Gusach, Anastasiia P-4
 Gensch, Thomas P-10
- H**
 Heinisch, Jürgen J. P-12
 Hsieh, Fu-Kai P-23
- I**
 Ishmukhametov, Aydar. OR-8, P-1, P-37
- K**
 Krupyanskii, Yurii OR-1
 Kamyshinsky, Roman OR-2, P-3, P-15, P-16, P-34, P-35, P-43
 Kulbatskii, Dmitrii S. OR-3
 Kocharovskaya, Milita V. OR-3
 Kirpichnikov, Mikhail P. OR-3, P-1, P-19, P-37
 Kralin, Vyacheslav A. P-3, P-35
 Kovalev, Kirill P-4
 Kudriavtsev, Aleksandr P-5
 Koo, Thomas M. P-8
 Kim, Young K. P-8
 Khorn, Polina P-10
 Karpova, M. P-11
 Karlova, Maria P-12, P-28
 Kotova, Elena Y. P-18, P-28
 Kniازهva, Anastasiia S. P-19
 Komarova, Galina A. P-19
 Kravchenko, Olesya V. P-20, P-27
 Khusainov, Iskander P-21, P-25
 Klochkova, Evelina P-21, P-26, P-31
 Kulakovskiy, Ivan V. P-22
 Koshkina, Daria P-24
 Korepanov, Alexey P. P-27
 Konevega, Andrey P-29
 Kolosova, Olga P-30
 Kartashev, Valery P. P-32
 Korshunova, Alena V. P-33, P-36
 Kostenko, Anastasiya P-34
 Kozlovskaya, Lubov P-37
 Kuklin, Alexandr I. P-38
 Kulabukhova, Darya G. P-43
 Korchevaya, Ekaterina P-44
 Kurochkina, Lidia P. P-45
 Krylov, Viktor P-47
 Kapranov, Ivan P-11
- L**
 Loiko, Nataliya OR-1
 Lyukmanova, Ekaterina OR-3
 Lisevich, Irina M. OR-4
 Lukianov, Dmitrii A. OR-4
 Luders, Jens OR-9
 Llorca Oscar OR-9
 Luginina, Aleksandra P-4
 Liu, Wei P-4
- Lozhnikov, Mikhail P-5
 Litvinov, Daniil P-14, P-46
 Landa, Sergey B. P-43
- M**
 Mozhaev, Andrey OR-2, P-13
 Marin, Egor P-4
 Mishin, Alexey P-4
 Maslov, Ivan P-10, P-17
 Malinina, Daria K. P-9
 Mishin, Alexander P-10
 Mulkidjanian, Armen Y. P-12
 Mileshina, Ekaterina P-13
 Maluchenko, Natalya P-24
 Maksimova, Elena M. P-27
 Myasnikov, Alexander G. P-27, P-27
 Mardonov, Djamsheed N. P-32
 Mamirov, Bahshillo R. P-32
 Makarova, Liubov O. P-36
 Moiseenko, Andrey P-37, P-41, P-46, P-47
 Molchanov, Vyacheslav S. P-38
 Morozova, Olga V. P-39
 Matveev, Vladimir V. P-42
 Maslova, Ekaterina S. P-45
 Miroshnikov, Konstantin A. P-46
- N**
 Nováček, Jiří OR-6
 Novoseletsky, Valery P-5, P-14
 Nesterov, Semen P-15
 Nurullina, Liliia P-21
 Novoseletskaya, Ekaterina S. P-41
 Nam, Ki Hyun P-4
- O**
 Orekhov, Philipp S. P-6
 Ognev, Aleksei V. P-7, P-8
 Osterman, Ilya OR-4
 Orekhov, Anton S. P-3, P-13, P-35, P-38
 Okhrimenko, Ivan P-40, P-11
- P**
 Popova, Anastasia V. P-46
 Přidal, Antonín OR-7
 Pichkur, Eugeny B. OR-8, P-13, P-29, P-45
 Philippova, Olga E. P-3, P-38, P-42
 Park, Jaehun P-4
 Papynov, Evgeniy K. P-7
 Petrenko, Alexander P-13
 Plokhikh, Konstantin P-15, P-34
 Putevich, Elena D. P-16
 Permyakov, Sergei P-17
 Paleskava, Alena P-29
 Palamarchuk, Konstantin P-34
 Pchelina, Sofya N. P-43
 Plevka, Pavel OR-6, OR-7
- R**
 Rogachev, Andrey V. P-38, P-40

- S**
Shtykova, Eleonora OR-2
Shenkarev, Zakhar O. OR-3
Sergiev, Petr V. OR-4
Smirnova, Tat'yana A. OR-5
Shevlyagina, Nataliya V. OR-5, P-39
Šiborová, Marta OR-6
Škubník, Karel OR-7
Sukeník, Lukáš OR-7
Samygina, Valeriya R. OR-8
Serna, Marina OR-9
Shaytan, Alexey K. P-1, P-5, P-19
Shaitan, Konstantin V. P-1, P-5, P-12, P-37
Shibaev, Andrey V. P-3, P-42
Sobirov, Mukhamad P-8
Samardak, Alexander S. P-7, P-8
Samardak, Aleksei Yu. P-7
Samardak, Vadim Yu. P-7, P-8
Sivkina, Anastasiia L. P-9, P-29
Studitsky, Vasily M. P-9, P-18, P-23, P-24, P-28
Strushkevich, N. P-11
Steinhoff, Heinz-Jürgen P-12
Sazonov, Dmitry A. P-16
Shtam, Tatiana A. P-16, P-43
Stetsenko, Artem P-21, P-30
Stolboushkina, Elena A. P-27
- Shulenina, Olga P-29
Shevchenko, Marina P-40
Selina, Daria V. P-41
Smirnova, Maria E. P-42
Samoilikov, Roman P-44
Shneider, Mikhail M. P-46
Shaburova, Olga P-47
Sokolova, Olga OR-1, P-12, P-14, P-28, P-37, P-41, P-44, P-45, P-46, P-47
- T**
Trifonova, Tatiana P-47
Tsarenko, Alexey P-40
- U**
Usachev, Konstantin P-21, P-25, P-26, P-30, P-31
- V**
Varfolomeeva, Elena Yu. P-43
Volokh, Olesya P-28
Vassilenko, Konstantin S. P-20, P-27
Vasiliev, Alexander L. OR-2, P-13, P-16
Vasilov, Raif P-15
Voskoboynikova, Natalia P-12
Vakhrameev, Daniil P-4
- Vorovich, Michail F. OR-8, P-1
Vácha, Robert OR-7
Van Raaij, Mark OR-6
Validov, Shamil P-25, P-26, P-30, P-31
- W**
Wang, Yueqi P-46
Weierstall, Uwe P-4
Wilson, Daniel N. OR-4
- Y**
Yunje, Cho P-4
Yaguzhinsky, Lev P-15
Yastremsky, Evgeny V. P-16
Yusupov, Marat P-25, P-26, P-30, P-31
Yakusheva, Alena P-29
- Z**
Zaigraev, Matvey M. OR-3
Zhukhovitsky, Vladimir G. OR-5, P-39
Zimmermann, Fabian OR-9
Zykov, Ilia P-17
Zernii, Evgeni P-17
Zgadzay, Yuriy P-30
Zagryadskaya, Yulia P-11, P-40
Zubarev, Ilya V. P-41
Zverev, Vitaly P-44